Closed-Loop Calibration of the Interaction Matrix for New Generation Adaptive Optics Systems:

A Least Cost Identification Approach

Fatih Han Çağlayan

Master of Science Thesis

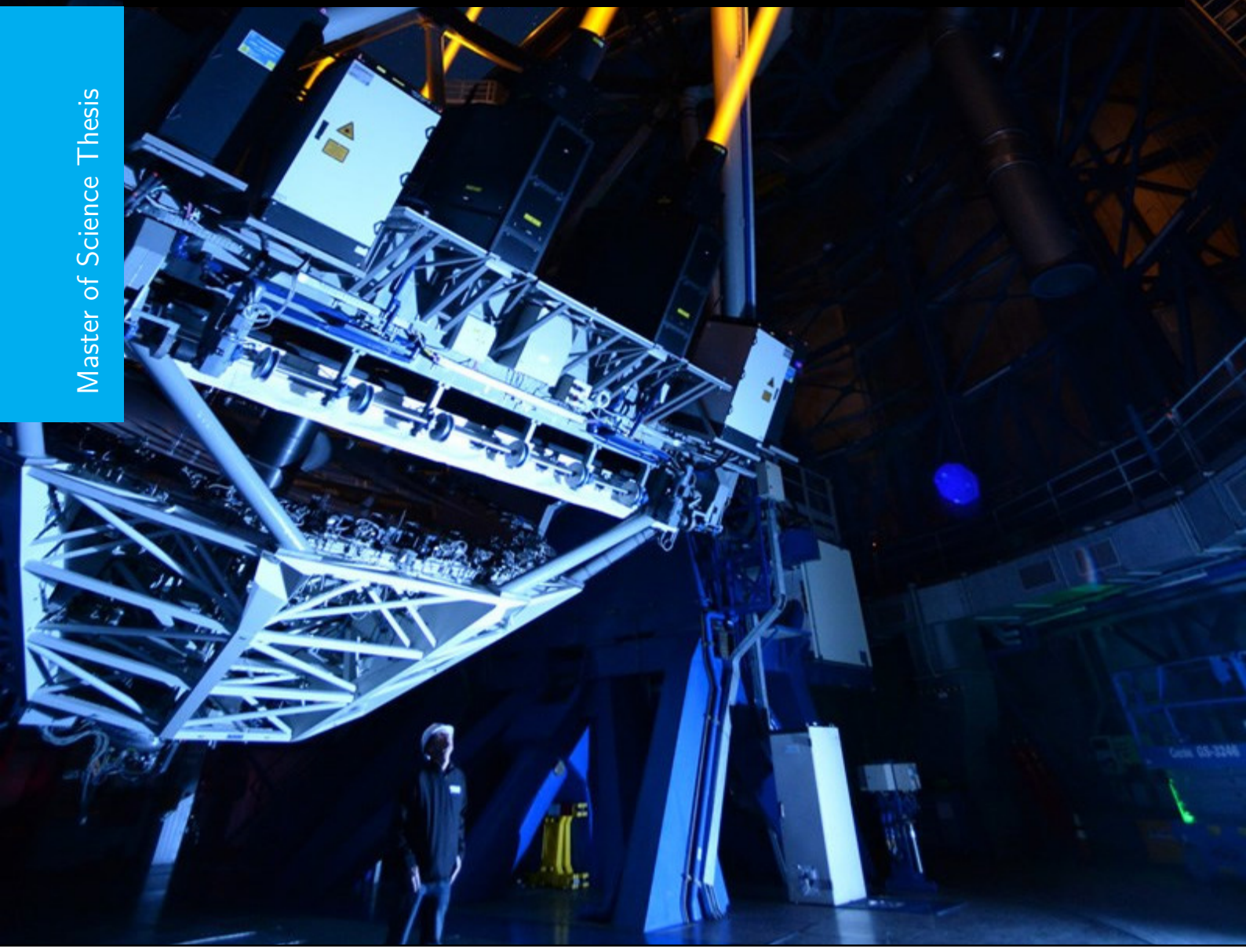

TU Delft Delft University of Technology

Delft Center for Systems and Control

Closed-Loop Calibration of the Interaction Matrix for New Generation Adaptive Optics Systems:

A Least Cost Identification Approach

Master of Science Thesis

For the degree of Master of Science in Systems and Control at Delft University of Technology

Fatih Han Çağlayan

August 16, 2017

Faculty of Mechanical, Maritime and Materials Engineering (3mE) · Delft University of Technology

The work in this thesis was supported by TNO Netherlands in Delft. Their cooperation is hereby gratefully acknowledged.

Abstract

Recently, with the switch to the new generation adaptive optics systems like the VLT and ELT an important identification problem emerged. These telescopes are so-called integrated systems, which means that open-loop calibration of the interaction matrix is not possible anymore. The first and foremost reason for this is that the new generation of integrated adaptive optics (AO) systems are much more sensitive to external factors like gravity causing misregistrations and system parameter changes. This sensitivity is due to the integrated design, because each time that the telescope will change from operation setup, such misregistrations will be created. Unfortunately, this can lead to performance loss or closed-loop instability very fast. Even misregistrations as big as 10% of a subaperture of the Shack-Hartmann wavefront sensor lead to significant performance loss.

For this reason, the identification and thereby correction for parameter changes in the deformable mirror (DM) have to be done during operation. Since the identification needs to be done during operation, it becomes much more important to have an identification method that does not disturb the closed-loop operation of the plant. Therefore, in this thesis, we will focus on a least cost method, preferably even a costless method for identification purposes.

Since the concept of integrated AO systems with a deformable secondary mirror (DSM) is still relatively new, there has been only one serious proposal for the solution of the problem by Béchet and Kolb. They falsely claim to have developed a non-parametric costless method, i.e. a method without excitation, for the calibration of the IM and achieved "reasonable" results.

In our work, we will first of all prove why their method is fundamentally wrong. Furthermore, we will also prove that their approach will result in the identification of the inverse controller instead of the plant. This is probably also the reason why they falsely suppose to have achieved "reasonable" results, because the dc gain of the inverse controller resembles the plant itself, which we will show as well.

After explanation and comparison of several methods, we will propose the recently developed least cost identification paradigm as the best solution. This paradigm is a framework for parametric prediction error identification and is meant to minimize the impact of the experiment on the underlying system in terms of experiment duration, distortion of the closed-loop

operation, power of the input signal or a combination of these, while at the same time guaranteeing a predefined level of accuracy. Different bottlenecks that need to be overcome to apply this method will be taken into account in order to adapt the least cost identification paradigm for the calibration of the interaction matrix (IM).

Using the expression for the information matrix we will first of all derive and proof that, theoretically, and if the experiment duration time allows, unlimited accuracy is achievable with zero cost in closed-loop using the excitation coming from the disturbance.

Furthermore, we will prove in our study that, when the cost is solely defined as the impact of the excitation signal on the normal closed-loop operation, the information-to-cost ratio per frequency is inversely proportional with the squared magnitude of the disturbance $H(\omega)$, i.e. proportional with $1/|H(\omega)|^2$. Therefore, this means that in our specific case, in which we try to find the static gain matrix for an underdamped second order resonance system with a low frequency disturbance originating from atmospheric turbulence, the Nyquist frequency will always be the optimal excitation frequency.

acknowledgements

This thesis is submitted in fulfillment of the degree of Master of Science in Systems & Control for the Delft Center for Systems and Control. All the work involved in finishing this thesis was carried out within the optomechatronics department of TNO in Delft, the Netherlands. TNO has offered me the chance to complete my thesis within their company by conducting this research. My motivation for this project was two-fold. Not only did I have the chance to apply my knowledge as a Systems & Control engineer in practice, but this was also a project that involved adaptive optics, which is my most favoured field practicing control due to the challenges faced.

Also it is important to note that this work could not have been established without the help of several people, who I would like to acknowledge here.

First of all, I would like to show my gratitude and appreciation to Professor Niek Doelman and Professor Michel Verhaegen. Prof. Doelman helped greatly on shaping the problem statement and provided wonderful supervision and assistance in TNO. Professor Michel Verhaegen provided technical supervision in the field of System Identification which is of course the main approach of this work.

Moreover, I would like to thank Wouter Jonker, the head of the optomechatronics department, for leading the projects and always supporting in time of need.

Finally, I would like to deeply thank my friends, parents and family, among which most notably my wife. They have always supported me in all different manners and have always been there for me when had my downs, but also they motivated me to aim even higher when I had my ups. My wife always gave me new insights and even helped me solve some important problems by listening to me no matter how difficult it was.

Delft, University of Technology — Fatih Han Çağlayan
August 16, 2017

Table of Contents

Chapter 1

Main introduction

In imaging systems, the diffraction limit is the fundamental limit that determines the possible quality [1]. However, in practice usually aberrations of the wavefront can also have a significant deteriorating effect on the reachable image quality [2].

In the case of Adaptive Optics (AO) with applications in astronomy, turbulence in the earthś atmosphere deteriorates the image quality of ground-based telescopes severely. The flat wavefronts that have originally traveled untouched for many light years get disturbed after reaching the earthś atmosphere. Through this, bright spots, so called speckles, occur on the image. Since these evolve very rapidly the image becomes blurry and smeared. Also, the earth's atmosphere causes the signal-to-noise ratio to drop.

Without atmospheric disturbance of the wavefront, the image quality limited by the diffraction limit improves linearly with an increase in the diameter of the telescope. Therefore, without a solution for this problem even the image quality of big telescopes like the ELT, which have a diameter of 39 m, would drop to the image quality of a telescope that has a diameter less than half a meter.

The simplest solution would be to build a satellite telescope and observe space by basically bypassing the source of the problem, which is the earth's atmosphere like it was the case with the Hubble telescope [3]. This also avoids the problem of limited transparency of the atmosphere, both temporal by clouds and in certain wavelength regions.

However, this method is not only very rigorous and complex, but also very expensive. Fortunately, the great advances in adaptive optics outperformed the quality of satellite telescopes when it was applied to ground-based telescopes [4].

Currently, there is an AO system in operation at almost every telescope larger than 4 m, but the developments have been so fast that there are numerous other applications as well. In Extreme Ultraviolet Lithography (EUVL) AO is suggested to correct for the heat deformations of the mirrors and lenses [5] [6]. For confocal and multi-photon microscopes the resolution of the images is severely affected by the changes in the refractive index of the observed object. In retinal imaging, the same problem occurs due to the fact that the eye is inhomogeneous which causes the refractive index to change based on location and time. The use of AO can

improve the imaging quality drastically by correcting for these type of aberrations [7] [8] [9] [10].

By now, it should be clear to the reader that AO plays a crucial role in numerous applications. For this thesis, we will focus on a problem that emerged recently with the switch to the new generation adaptive optics systems like the VLT and ELT. These telescopes are so-called integrated systems, which means that open-loop identification of the interaction matrix, which is also called calibration, is not possible anymore. Therefore, closed-loop identification has to be done while the telescope is under operation.

The basic idea behind AO is that the phase differences in the wavefront created through the atmospheric turbulence get corrected by a deformable mirror (DM). In this process, the Interaction Matrix (IM) plays a crucial role, because it relates the commands sent to the mirror with the shape that the DM obtains.

The identification of the IM, which is also called the calibration of the IM in the field of AO, is therefore an important task. Not only are the new generation of integrated AO systems like the VLT and ELT much more sensitive to misregistrations of the IM, but also the identification must be done in closed-loop while the telescope is active, because open-loop identification is simply not possible anymore.

For identification, some form of excitation is needed. However, excitation also means degradation of the imaging performance. ESO would like to be able to perform imaging without any interruption or disturbance. For this to be possible, it is needed to calibrate the IM when the setup of the telescope changes.

Therefore, the identification method should guarantee low disturbance of the imaging performance while at the same time being sufficiently rich to identify a correct IM. Defining the imaging performance in terms of the imaging quality and experiment duration will be another part of the research.

1-1 Problem definition

With the emergence of the new generation AO systems which utilize a Deformable Secondary Mirror (DSM), such as the ELT and the VLT of ESO, closed-loop calibration has become necessary. Therefore, the identification experiment will be during operation. This is also the reason why a low cost or preferably even a no cost identification method for calibrating the Deformable Mirror of the telescope.

In the following subsection, we will explain more elaborately, why it is necessary to calibrate the DM in closed-loop and why this creates the need for a low cost method.

1-2 Why is a least cost closed-loop identification approach necessary?

Let us first address the question of why we have to identify the DM of the new generation AO systems with a DSM in closed-loop during operation. For the older generation of telescopes with conjugate-plane DM, an open-loop identification is already sufficient. This is due to the

separation of the DM from the actual AO system. The dynamics do not change drastically during operation and identification during operation is redundant. So the identification can be done as shown in Figure 1-1a.

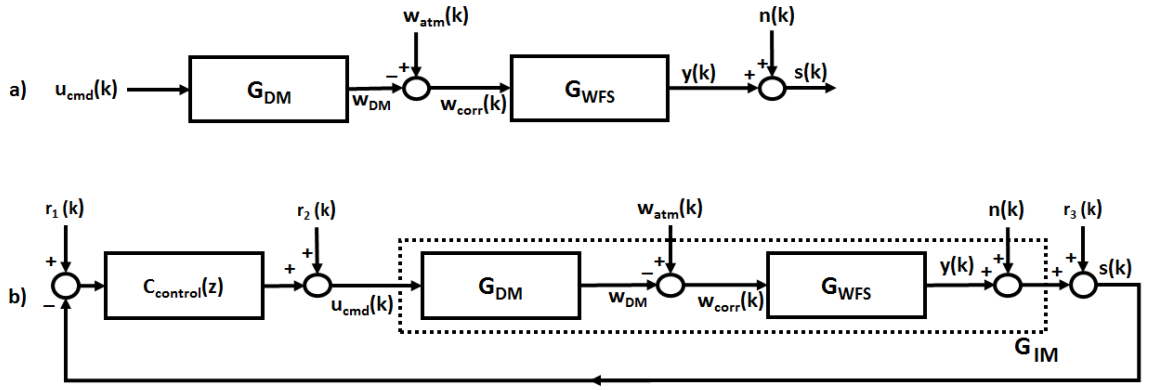

Figure 1-1: *a:* Open-loop setup for identification *b:* Closed-loop setup for identification

The need for identification during operation emerged quite recently with the switch to the new generation AO systems with a Deformable Secondary Mirror, which is integrated into the system. For the reason that these systems are integrated, open-loop identification as shown in Figure 1-1a is physically not possible anymore. Therefore, we have to identify these type of telescopes according to the setup as shown in Figure 1-1b.

One might, now, still raise the question: *"So what is the problem? Why is simply performing a closed-loop calibration not enough?"*.

The first and foremost reason is that the new generation of integrated AO systems are much more sensitive to external factors like gravity causing misregistrations and system parameter changes. This sensitivity is due to the integrated design, because each time that the telescope will change from operation setup, such misregistrations will be created. Unfortunately, this can lead to performance loss or closed-loop instability very fast [11] [12]. Even misregistrations as big as 10% of a subaperture of the Shack-Hartmann wavefront sensor lead to significant performance loss [11]. This is the reason why identification a priori is not of much use, because we want to correct for parameter changes in the DM by updating the IM *during operation*.

The answer to our first question, also partially answers the second question; the identification has to be done during operation. Obviously, scientists will not want their observations to be distorted by excitation needed for identification. On the other hand, the identification is needed to be able to produce observations in the first place. This is also where a difficult trade-off comes into picture. The accuracy of the identification will be larger when the excitation signal is larger, but this also holds for the degradation of the imaging quality due to the same excitation signal. Therefore, we want to design an identification experiment that guarantees a predetermined accuracy while doing this at the lowest possible cost.

The challenge lies also in defining the cost for different types of observations. One can imagine that, depending on the type of observation, the cost will be defined differently. The method might give weights to certain frequencies according to how much they would degrade the performance of the system. It might also be a trade-off between experiment duration and accuracy. One might choose for low-impact combined with a long duration or vice versa.

1-3 Research objectives

The main research objective for the Thesis is to provide control theoretically supported methods for least cost identification of the DM of integrated AO systems. In our case, the Deformable Secondary Mirror (DSM) of the AOF will be considered especially. The main research question can be formulated as follows:

"How can we perform least cost identification of the DM of the new generation integrated AO systems where the cost can be defined as the experiment duration and deterioration of the image quality due to the experiment?"

This main research question can be divided into sub-questions as follows

- How does atmospheric turbulence effect the imaging quality and how do AO systems try to counteract this?
- How can we simulate the sensor and control signals of an AO system in a closed-loop setting for realistic representation of the performance of proposed methods?
- What type of least cost identification methods can be applied to the AO system in question
  - Is it possible to identify the DSM in closed-loop without explicit external excitation by only using the excitation coming from the atmospheric turbulence?
  - If we consider that the measurement noise is negligible in practice, or mathematically even zero, how can we apply least cost identification without considering the deterioration of image quality?
  - How can we translate the requirements on the imaging quality to requirements that can be used when optimizing the identification experiment.
  - When the deterioration of the imaging performance in terms of imaging quality and experiment duration are taken into account, how can we apply least cost identification.

1-4 Thesis outline

The theoretical background of this research is contained in Chapters 2 and 3, which can be read independently. In Chapter 2, a brief introduction to and a summary of atmospheric turbulence and adaptive optics will be presented. Finally, the separate elements that make up an AO system will be discussed and a control-theoretical model of such an AO system will be discussed. In Chapter 3, an overview will be given of the state of the art methods to solve our method. In this Chapter, we will discuss the single proposed solution to our problem by Béchet and Kolb and proof why it is fundamentally wrong. Furthermore, the fundamentals of parametric prediction error identification and a recently developed least cost identification paradigm will be discussed. Mainly this Chapter will provide the theoretical support to the results presented afterwards.

In Chapter 4, we will form a research proposal based on our study of the state of the art. We will shortly mention that we cannot use the method proposed by Béchet and Kolb simply because it is fundamentally wrong. A proof of principle will be given for costless identification, i.e. identification without explicit external excitation, and for the cases in which explicit external excitation is necessary, we will formulate how we would like adapt the least cost identification paradigm to our problem at hand.

Chapters 5 and 6 are devoted to our research and the corresponding results. In Chapter 5, we will mainly focus on how to apply least cost identification. We will mention the roadblocks that need to be overcome and several important considerations during our research are mentioned. One of the most important considerations is the parametrization of the excitation signal. We have for example applied a sinusoidal parametrization of the excitation signal instead of an FIR parametrization as applied in the literature of the least cost identification paradigm. Furthermore, in the same Chapter, we will dwell on the capabilities of costless identification, and we will prove that the disturbance H does not affect the amount of information in any way, but instead, solely depends on the controller C and the plant G. In Chapter 6, the resulting least cost excitation spectra for three different representative models of AO systems will be presented. At the end of the Chapter, we will derive mathematically that the single frequency information-to-cost ratio for second order resonance systems in general is proportional with the inverse squared magnitude of the disturbance. This means for our system at hand, in which we are dealing with atmospheric turbulence, that has the character of low pass filtered disturbance, the Nyquist frequency will always be the optimal frequency.

The prefinal Chapter 7 will contain a discussion and evaluation of our applied method. In this context we will also give recommendations for further research based on our discussion.

Finally, our conclusion will be presented in Chapter 8.

Chapter 2

Atmospheric turbulence and adaptive optics systems

This chapter will provide an introduction to the concepts of atmospheric turbulence and adaptive optics. We will start by describing and modeling atmospheric turbulence after which we will discuss how AO systems counteract this phenomenon. The last part will especially discuss how a wavefront is measured and reconstructed.

2-1 Atmospheric turbulence

In the atmosphere small temperature variations occur which in turn cause local changes in wind velocity, so called eddies. This is viewed as turbulence in the atmosphere. Since the rise in temperature also changes the atmospheric density, the refraction index is also changed. These local changes accumulate and can cause significant inhomogeneities in the refraction index at different locations in space and time. These small changes in the refraction index disturb incoming wavefronts [13]. In this section we will describe how physical models for atmospheric turbulence are obtained and how this affects the wavefront.

2-1-1 Physical model of atmospheric turbulence

Based on the work of [14], [15] and [16], the refraction index in atmosphere can be assumed to consist of two parts $\langle n(\mathbf{r})\rangle$, which is the mean refraction index and $\langle n_1(\mathbf{r})\rangle$, which can be seen as the fluctuating part of the refraction index. The covariance Cov_{atm} of the refractive index then becomes [13]:

$$Cov_{atm} = \langle n_1(\mathbf{r} + \mathbf{r1})n_1(\mathbf{r1})\rangle \tag{2-1}$$

The power spectral density (PSD) can be calculated by taking the Fourier transform of the above described covariance:

$$\Phi_n(\mathbf{K}) = \frac{1}{8\pi^3} \int d^3\mathbf{r} Cov_{atm}(\mathbf{r}) e^{-i\mathbf{K}\cdot\mathbf{r}}, \tag{2-2}$$

where $\mathbf{K}$ is the three-dimensional spatial wave number. Changing to spherical coordinates with $\mathbf{K} = (k, \theta, \phi)$ and rearranging gives:

$$\Phi_n(k) = \frac{5}{18\pi} C_n^2 k^{-3} \int_{l_0}^{L_0} dr sin(kr) r^{-1/3}, \tag{2-3}$$

where C_n^2 is the structure constant which represents the turbulence at each position in the propagation. The large eddy, the so called outer scale, is L_0, which is the size above which isotropic behavior is violated. The small eddy l_0, the so called outer scale is the size below which viscous effects are important and energy is dissipated into heat [13].

Kolmogorov proposed to let the limits of the integral diverge for simplified integration, $l_0 \to 0$ and $L_0 \to \infty$ [15]:

$$\Phi_n(k) = 0.033 C_n^2 k^{-11/3} \tag{2-4}$$

A spectrum with finite outer scales is given by Von Karman expressed in frequency instead of wave number [17]:

$$\Phi(f, z) = 0.033 C_n^2(z)(f^2 + f_0^2)^{-11/6} e^{-f^2/f_i^2}, \tag{2-5}$$

2-2 Disturbance of the wavefront due to turbulence and adaptive optics

As we have seen in the previous Section, the atmosphere causes the flat wavefront to be disturbed. This can be corrected by using an AO system which is depicted schematically in Figure 2-1. Flat wavefronts from space come into the atmosphere of the earth and are distorted. The light is captured by a telescope and analyzed by a wavefront sensor. How this works is described in the following Subsection. After reconstructing the wavefront through the local slopes at different locations of the incoming wavefront, the idea is to use a Deformable Mirror (DM) to produce the exact opposite of the distortion. Actuators are used to deform the DM and in that sense it can be viewed as a membrane.

Mathematically, we can use the following notation for the wavefront in phasor notation φ:

$$\varphi(\mathbf{r}, t) = e^{\phi(\mathbf{r}t)}, \tag{2-6}$$

where $r \in \mathbb{R}^2$ denotes the spatial position in the telescope and t denotes the time. For a flat wavefront, it should hold that $\varphi(\mathbf{r}, t) = 0$. The goal of the AO system is to correct for the distortion by bringing $\varphi(\mathbf{r}, t)$ as close as possible to zero.

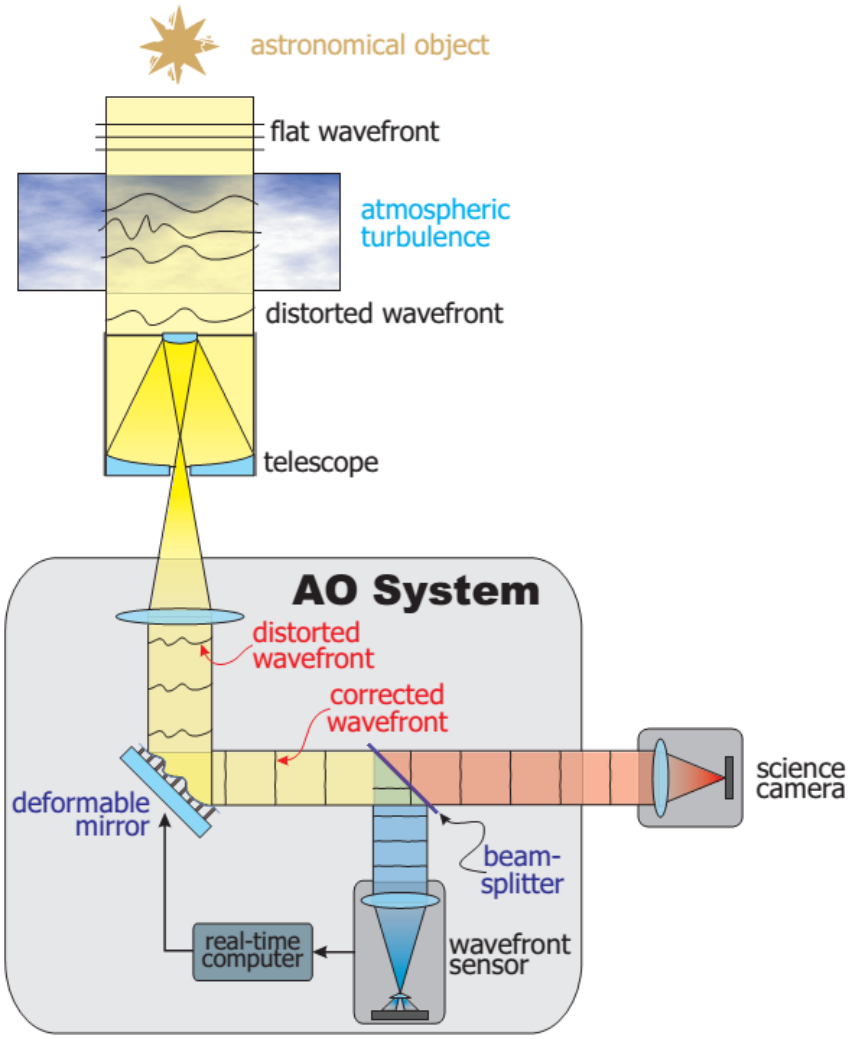

Figure 2-1: Principle of Adaptive Optics adapted from [18]

2-2-1 Wavefront sensing

An adaptive optics system needs to be able to determine and reconstruct the wavefront in order to correct for aberrations. There are multiple methods available for wavefront sensing such as the Shack-Hartmann sensor [19], the curvature sensor [20] and pyramid sensor [21]. For this thesis, only the Shack-Hartmann sensor will be relevant due to the fact that the systems involved all use a Shack-Hartmann sensor. In this Section, we will describe the development and working principle of the Shack-Hartmann sensor.

Hartmann sensor

In 1900 Johannes Franz Hartmann developed a test for lenses or mirrors [22] [23]. The idea is to put an opaque mask with uniformly distributed holes behind the lens or mirror. Since all the holes act as an aperture, an image of spots will be produced. Thereby the wavefront

is actually sampled and locally estimated by a first order approximation. In the case of a plane wave, the spots will be uniformly distributed over the image plane, while in the case of another shape wavefront, the spots will diverge accordingly. The working principle of the Hartmann test is depicted in Figure 2-2

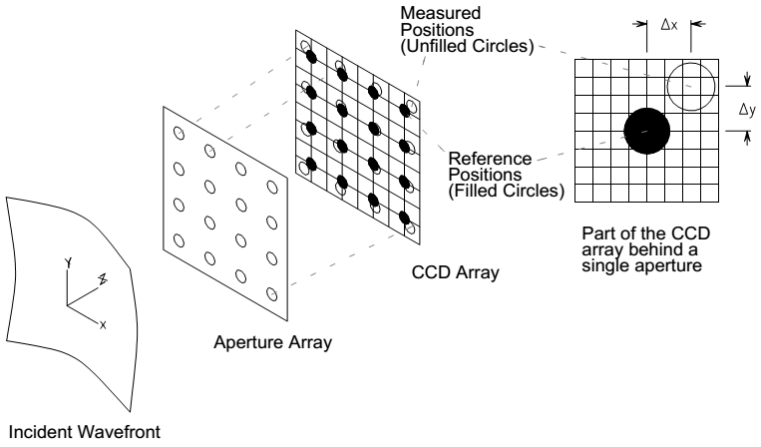

Figure 2-2: Working principle of the Hartmann Test adapted from [24]

Shack-Hartmann sensor

Although, the idea of the Hartmann sensor was very good, it still had some major problems. The images were of low intensity and thereby more noise problems occurred. Furthermore, the holes caused disturbing diffraction effects. In 1971, Roland Shack and Ben Platt replaced the aperture array by a lenslet array [19]. This would solve both of the important problems that the Hartmann sensor had. The working principle is basically the same as the Hartmann sensor and is depicted in Figure 2-3.

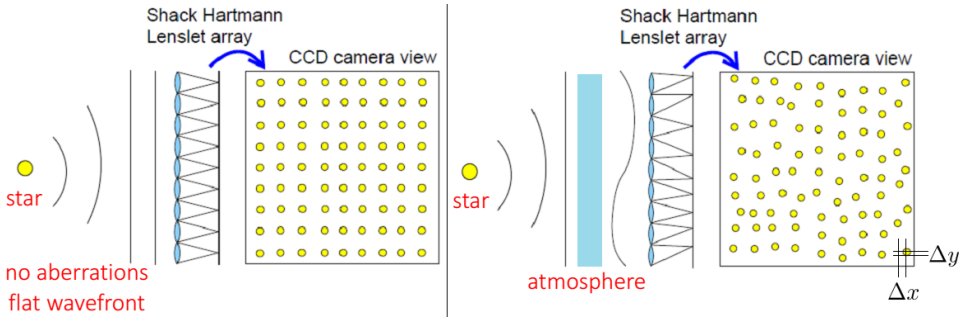

Figure 2-3: Working principle of the Shack-Hartmann wavefront sensor adapted from [2]

The array of lenslets samples the wavefront, after which the local sample is approximated by a first order estimate. The local slope is found from the spot deviation. This will be explained in the next part.

Spot deviation and local wavefront slope

In this part, we will explain how the spot deviation in the image plane, most probably a CCD

sensor, relates to the local slope of the wavefront. For this explanation, Figure 2-4 will be used as a reference.

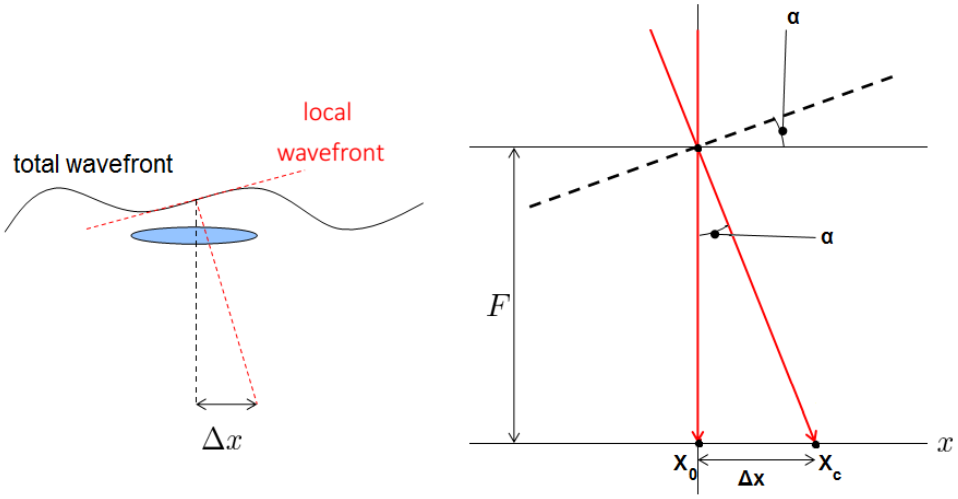

Figure 2-4: How a disturbance in the wavefront translates into deviation of the spot

The derivation will be done for a one dimensional representation, the x-coordinate. The derivation for the two-dimensional case is similar.

First of all we will need to determine the spot center. In the case of a CCD sensor this can be done by means of the center of gravity method:

$$x_c = \frac{\sum_{i,j} x(i,j)I(i,j)}{\sum_{i,j} I(i,j)}, \tag{2-7}$$

where x(i,j) denotes the x-coordinate of the corresponding pixel on the CCD. The spot deviation can then be found by subtraction $\Delta x = x_c - x_0$. The angle of arrival α_x, in Figure 2-4 depicted as α, can be found as follows:

$$\alpha_x = \frac{\Delta x}{F}, \tag{2-8}$$

where F is the focal distance the lens. In the case of the Hartmann sensor, the angle of arrival would directly represent the local slope s_x:

$$s_x = \frac{\partial \phi(x,y)}{\partial x} = \alpha_x \tag{2-9}$$

However, in the case of the Shack-Hartmann sensor, we have to keep in mind the lens which changes the angle of arrival. Therefore, the local slope in the case of a Shack-Hartman sensor can be found as follows:

$$s_x = \frac{\partial \phi(x,y)}{\partial x} = \frac{2\pi d \alpha_x}{\lambda} \tag{2-10}$$

2-2-2 Wavefront reconstruction

After obtaining the local slopes from the Shack-Hartmann sensor, now rests the determination of the phase. This is called wavefront reconstruction and is one of the fundamental problems in adaptive optics [25]. The problem can be summarized by the following Equation:

$$s = B\phi(x, y), \tag{2-11}$$

where B is called the geometry matrix. This matrix depends on chosen the method. Note that noise from the Shack-Hartmann sensor has not been taken into consideration yet.

The easiest method for this is based on direct least-squares methods [26] [25] which transform the problem basically into a finite difference method. These are called zonal reconstruction methods. For the Fried method, the slopes from the Shack-Hartmann sensor are related as follows to the phase:

$$s_x(i,j) = \frac{(\phi(i+1,j) + \phi(i+1,j+1))/2 - (\phi(i,j) + \phi(i,j+1))/2}{w}, \tag{2-12}$$

$$s_y(i,j) = \frac{(\phi(i,j+1) + \phi(i+1,j+1))/2 - (\phi(i,j) + \phi(i+1,j))/2}{w}, \tag{2-13}$$

where w represents the distance between the center of the lenslets in the arranged array in the sensor. These equations can be written in matrix form as follows:

$$s = B\phi(x, y) + \eta, \tag{2-14}$$

where η represents the noise from the Shack-Hartmann sensor. The phase $\phi(x, y)$ can be found by solving the equation above.

Zonal methods basically sample the continuous plane of the wavefront after which they use a locally first order approximation. The whole plane is then represented by the sum of these first order representations. This is a proven method and for the purpose of this thesis we will use this for wavefront reconstruction

Alternative methods have been proposed for wavefront reconstruction such as the method of Southwell, which represent the continuous plane of the wavefront by a polynomial expansion [27]:

$$\phi(x, y) = \sum_{k=1}^{K} a_k Z_k(x, y) \tag{2-15}$$

More recent methods such as [28] [29] [30] [31] have been developed as well. These focus mainly on reducing the needed computational effort by means of simplifying the algorithm or by means of parallelization.

2-3 Control-theoretical model of an adaptive optics system

It is important to make the necessary abstractions to the system shown in Figure 2-1. Therefore, we will define the AO system that we are dealing with in a control-theoretical context. We will start by a block diagram representation of our system followed by a discussion of the separate elements.

In Figure 2-5, the block diagram representation of a closed-loop AO system can be found. The different parts in Figure 2-1 have been abstracted to control blocks.

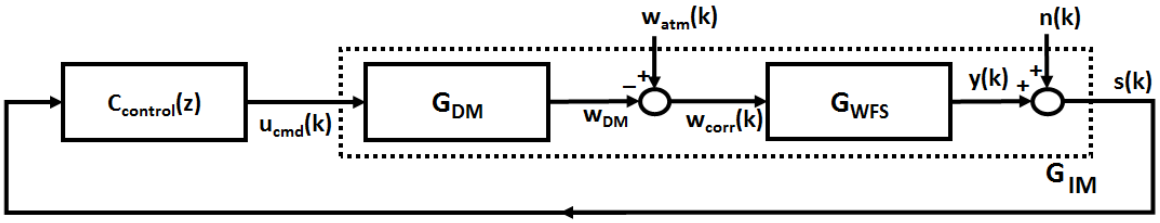

Figure 2-5: Block diagram representation of an AO system

A representation in equation form is also important from an analysis point of view. The closed-loop AO system can be modeled by the following set of equations:

$$s(k) = \mathfrak{S}(w_{atm}(k)) - G_{IM} \cdot u_{cmd}(k) + e(k) \tag{2-16}$$

$$u_{cmd}(k+\tau) = u_{cmd}(k-1+\tau) + \gamma G_{IM}^{+} \cdot s(k) \tag{2-17}$$

The control blocks and signals in Figure 2-5 and the equation above will be discussed below:

Atmospheric turbulence: $\mathbf{w_{atm}}$ The telescope has a disturbance input that is coming from the atmosphere as discussed earlier. This is named $w_{atm}(k)$ and it is a continuous representation of the turbulence in the atmosphere at the time of sample k. The spectrum of the disturbance is important from a control-theoretical perspective and both the Kolmogovorov and Von Karman atmospheric turbulence spectra can be found in Figure 2-6.

The function $\mathfrak{S}$ The continuous turbulence representation w_{atm} is transformed into a discrete set of data by the function $\mathfrak{S}$. The size of $\mathfrak{S}(\mathfrak{w}_{\mathfrak{atm}})$ depends on the number of lenslets of the Shack-Hartmann sensor and is the same as the size of $s(k)$.

Deformable Mirror: DM The Deformable Mirror DM is in this case the part that is of most interest for us, the part that we eventually want to identify. In literature, the DM is usually modeled as a simple MIMO gain [11] [12] [13] [32]. The reason why this is possible can be understood by comparing Figure 2-7 with Figure 2-6. In the active range of the spectrum of atmospheric turbulence the DM can indeed be viewed as a MIMO gain and therefore all the dynamics can be left out in the modeling. This is then called the Interaction Matrix (IM). The spectrum in Figure 2-7 is the transfer function from actuator 1 to slope 1 for the Deformable

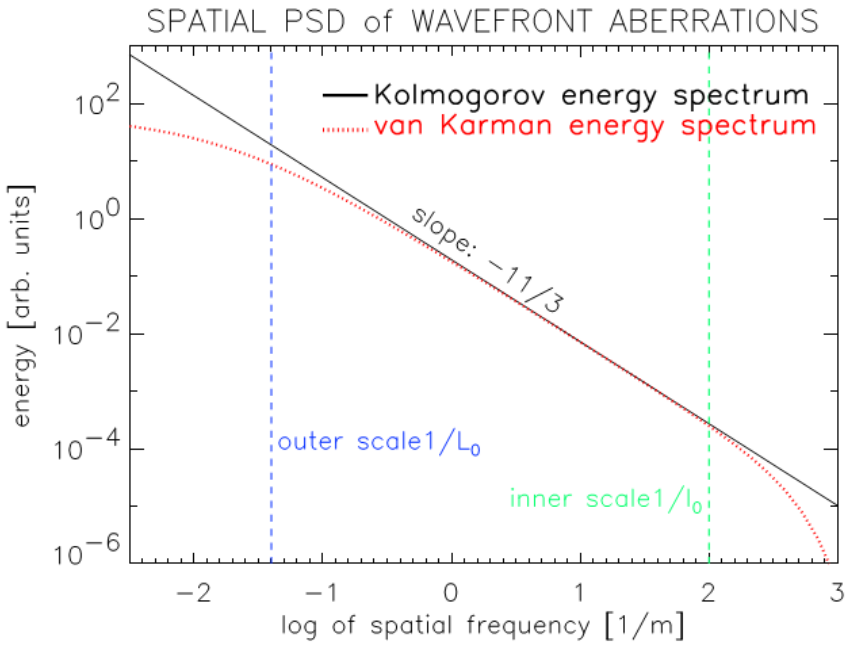

Figure 2-6: A 1-D cross-cut of the spatial spectrum of atmospheric turbulence adapted from [18]

Secondary Mirror (DSM), an integrated type of deformable mirror. Although the transfer function will look different for other actuators and/or slopes, in general we can assume that the transfer function from the actuator to the slope of any DM for any type of telescope will have a similar shape. In that sense, it is very comparable to that of a mass-spring-damper system.

Controller: $\mathbf{C_{control}(z)}$ The controller $C_{control}(z)$ is a combination of a pure integrator and the so called Command Matrix, which is the pseudoinverse of G_{IM}. It can be described by the following equation:

$$C_{control}(z) = \frac{\gamma}{1 - z^{-1}} G_{IM}^{+}, \tag{2-18}$$

where G_{IM}^{+} is the pseudoinverse of G_{IM}.

Actuator input commands: $\mathbf{u_{cmd}(k)}$ The DM command vector applied at time k is called $u_{cmd}(k)$. The length of this vector depends on the number of actuators that the DM in question has.

Shack-Hartmann sensor: WFS-SH The Shack-Hartmann wavefront sensor basically samples the incoming continuous wavefront and has as outputs the slopes of the wavefront. The sensor should be sensitive enough in order to be able to observe all modes of the system. Otherwise, it is possible that additive noise will destabilize the system without actually noticing it.

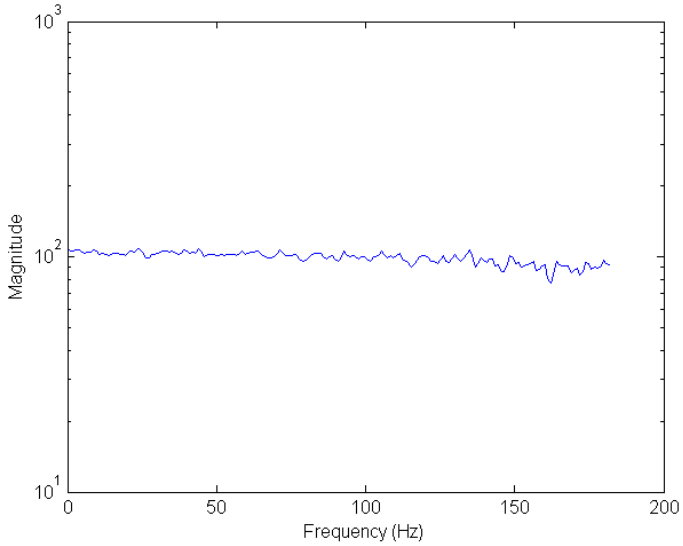

Figure 2-7: The transfer function from actuator 1 to the 492nd slope in x for the DM of the VLT

Shack-Hartmann output slopes: $\mathbf{s(k)}$ The vector $s(k)$ contains the x- and y-slopes coming from the wavefront sensor at time k. The continuous wavefront is then represented by a set of slopes. The Shack-Hartman sensor should have more apertures than actuators in the DM.

Measurement noise: $\mathbf{e(k)}$ The output measurement noise at time k is represented by the vector $e(k)$. This is added to the output $y(k)$. So the final output $s(k)$ that comes from the sensor is as follows:

$$s(k) = y(k) + e(k) \tag{2-19}$$

AO system delay: τ It takes a finite amount of time for the sensor to capture photons and for the system to process the incoming data. Therefore, each system has a certain delay. This is called the AO delay τ and is represented in the number frames.

2-4 Simulation of an adaptive optics systems

Since we do not have an actual system at our disposal, AO research is best done by means of simulation. This will give us the opportunity to analyze the performance of the existing identification schemes and algorithms and compare it to the performance of the identification schemes that we will develop for closed-loop identification. The overall simulation system will be designed in Matlab. This Section will describe how different parts of the system have been modeled in our simulation system.

2-4-1 System parameters of the simulated adaptive optics telescope

For the purpose of simulating an AO system, we chose a square DM that has size 0.99 m by 0.99 m. The DM will have 11 by 11 actuators making a total of 121 actuators. The Shack-Hartmann sensor will have 32 by 32 lenses, thereby resulting in a total 2048 slopes.

Turbulent atmosphere $w_{atm}(k)$ will move over the telescope. This "turbulence carpet" that is 0.99 m by 655.36 m will move with a wind speed of $v = 10\ m/s$ over the square aperture of the telescope. It has more samples than needed by the Shack-Hartmann to replicate the effect of going from a continuous representation of a distorted wavefront to a sampled output by the Shack-Hartmann sensor. The "turbulence carpet" is a cutout of a square field turbulence that was originally 655.36 m by 655.36 m. How this was modeled can be read in the following Section.

A sampling frequency of $f_s = 1\ kHz$ will be applied for our simulated AO system. The system delay τ equals 2 samples, and the noise e(k) can be chosen with an arbitrary mean according to the simulation that is needed. A gain of $\gamma = 0.8$ was chosen for the integrator. The whole system can, therefore, be modeled according to Equation 2-16 as follows:

$$s(k) = \mathfrak{S}(w_{atm}(k)) - G_{IM} \cdot u_{cmd}(k) + e(k) \tag{2-20}$$

$$u_{cmd}(k+2) = u_{cmd}(k+1) + \gamma \cdot G_{IM}^{+} \cdot s(k) \tag{2-21}$$

where $s(k) \in \mathbb{R}^{2048\times 1}$, $\mathfrak{S}(w_{atm}) \in \mathbb{R}^{2048\times 1}$, $G_{IM} \in \mathbb{R}^{2048\times 121}$, $u_{cmd}(k) \in \mathbb{R}^{121\times 1}$, $e(k) \in \mathbb{R}^{2048\times 1}$, $G_{IM}^{+} \in \mathbb{R}^{121\times 2048}$

2-4-2 Modeling atmospheric turbulence for simulation

The exact modeling of atmospheric turbulence for the simulation can be found in Appendix A.

Chapter 3

System identification: state of the art

This Chapter will present an overview of the existing system identification methods that can be applied to our system in question and discuss their properties. The goal is to provide the reader with the necessary instruments and theoretical knowledge for identification purposes.

We will first discuss a novel and supposedly costless method for identification proposed by Kolb and Béchet in [11] and [12]. A proof will be given why this method is fundamentally incorrect, and we will show that actually the inverse controller is identified instead of the plant itself. After this, we will continue with the explanation of parametric identification. For all cases, we will start from the open-loop case and then extend the method to closed-loop. Each time, we will refer to Figure 3-1a or Figure 3-1b respectively. Finally, we will present the concept of least cost identification, which is recently developed by Michel Gevers.

3-1 Supposedly costless closed-loop identification proposed by Kolb and Béchet

Kolb and Béchet proposed a supposedly no-cost closed-loop identification method in [11] and [12]. In the following Section, it will be shown that costless identification is only possible for parametric methods when certain requirements are met. It is a well-known fact that using direct spectral identification, i.e. using the plant input $u(k)$ and the output $y(k)$, will lead to identification of the inverse controller [33]. Since the method proposed by Kolb and Béchet is nonparametric [11] [12], it cannot possibly work. Furthermore, also no model for the disturbance coming from the atmospheric turbulence is taken into account in [11] and [12]. Therefore, even for a parametric method it would have been impossible to work.

However, Kolb still claims to have achieved "promising results" [11]:

"Measurements and commands with apparently no other structure than the one of the turbulence actually lead to a reconstructed IM very similar to one measured on a fiber, but with a lower SNR"

In the follow-up, however, he continues [11]:

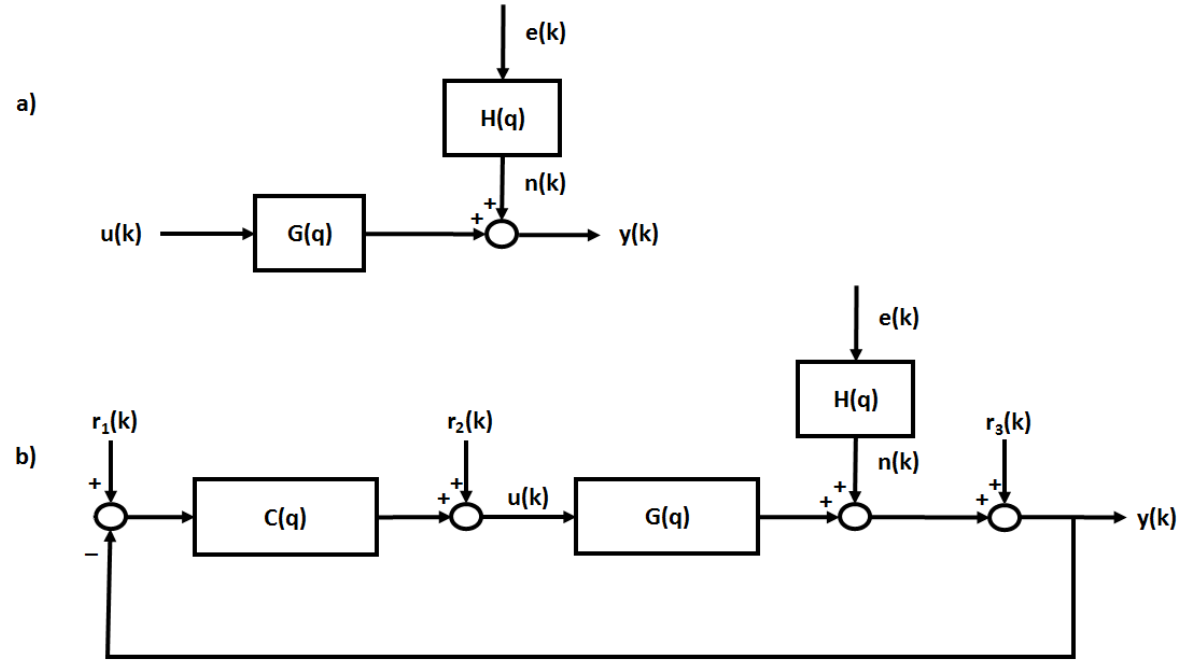

Figure 3-1: General configurations for *(a)* open-loop and *(b)* closed-loop identification purposes

"Although the quality of this IM is too poor to be used in order to efficiently close the loop, it is enough to retrieve a few misregistration parameters."

3-1-1 Explanation of the method of Kolb and Béchet

For explanation of their method we will use Figure 3-2 as a reference. It is clear that the plant input $u(k)$ is correlated with the disturbance $w_{atm}(k)$. The very first, incorrect, assumption in [11] and [12] is that we can get rid of this correlation by taking increments of the inputs and outputs:

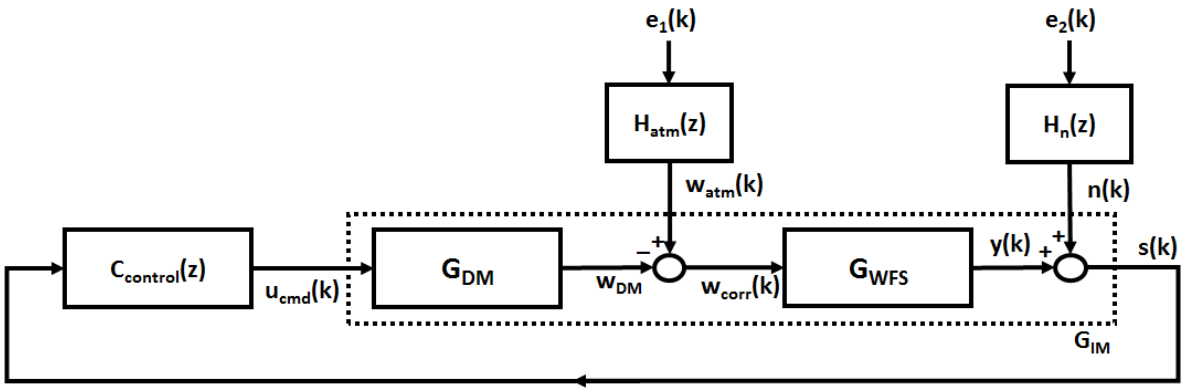

Figure 3-2: Configuration for closed-loop identification as explained by [11] and [12]

$$\delta u(k) = u(k) - u(k - \Delta k), \tag{3-1}$$
$$\delta s(k) = s(k) - s(k - \Delta k), \tag{3-2}$$

where Δk is a predetermined number of samples. They claim that selecting several sets of incremental measurements separated by a certain number of frames Δk can get rid of the correlation if Δk is chosen large enough. First, let us address the correlation issue; **it is impossible to get rid of the correlation by means of filtering**. The single source of excitation in the system as shown in Figure 3-2 is the atmospheric disturbance. Therefore, the very existence of the input $u(k)$ depends on the existence of $s(k)$, which on its turn depends on the existence of the disturbance $w_{atm}(k)$. The correlation of the input with the disturbance will be explained mathematically in the following Subsection. Clearly, taking differences of any sort will not get rid of this correlation, because the very same argument also holds for the incremental differences: if there would be no incremental differences in $s(k)$, there would be no incremental differences in $u(k)$ and vice versa. This clearly shows the correlation between the input and the output. Also, let us analyze the so called incremental differences actually mean. This is basically nothing more than filtering the input and output data by the following filter, which is nothing more than a high-pass filter:

$$L(q^{-1}) = \frac{1}{1 - q^{-\Delta k}} \tag{3-3}$$

Applying this filter can at most get rid of some noise, but will not change the final result. Therefore, in a situation without noise, it is possible to apply the algorithm with the unfiltered input-output data.

$$G^*_{IM} = -s \cdot u^+_{cmd} \tag{3-4}$$

3-1-2 Fundamental problem in the method of Kolb and Béchet

Qualitatively, it is already clear that the mentioned assumption is incorrect. Let us now analyze this more mathematically to understand what is fundamentally wrong with the approach as mentioned in [11] and [12]. For Gaussian noise n, we know that the following holds true:

$$R_{nn}(\tau) = \begin{cases} \sigma^2 \delta(\tau), & \text{if } \tau = 0 \\ 0, & \text{otherwise} \end{cases} \tag{3-5}$$

For systems in which a pure Gaussian white noise sequence n is the single source of excitation. The assumption of Kolb and Béchet holds true, because in that case clearly $E[u(k)n(k)] = 0$.

However, not only is it impossible to realize pure Gaussian white noise in practice, but most importantly, in this case, we are dealing with atmospheric turbulence and not with pure Gaussian white noise. For disturbance coming from atmospheric turbulence it simply does not hold that $R_{w_{atm}w_{atm}}(\tau) = 0$ when $\tau \neq 0$. Therefore, the expectation of the input and disturbance will be nonzero, i.e., $E[u(k)n(k)] \neq 0$, which in turn means that the input is

correlated with the disturbance. For this reason, the very first assumption of Kolb and Béchet breaks down and the remaining method, thus, does not hold.

So let us understand what will be the result of the method of Kolb and Béchet instead. For this purpose, we will look back at Figure 3-2 and derive the equations for the output $s(k)$ and the input $u(k)$, the arguments will be left out for brevity:

$$s = \frac{G_{WFS}H_{atm}e_1 + H_n e_2}{1 + G_{WFS}G_{DM}C} \tag{3-6}$$

$$u = \frac{CG_{WFS}H_{atm}e_1 + CH_n e_2}{1 + G_{WFS}G_{DM}C} \tag{3-7}$$

From the above equations the following spectral densities follow:

$$\Phi_{su} = \frac{C|G_{WFS}|^2|H_{atm}|^2\Phi_{e_1} + C|H_n|^2\Phi_{e_2}}{|1 + G_{WFS}G_{DM}C|^2} \tag{3-8}$$

$$\Phi_{uu} = \frac{|C|^2|G_{WFS}|^2|H_{atm}|^2\Phi_{e_1} + |C|^2|H_n|^2\Phi_{e_2}}{|1 + G_{WFS}G_{DM}C|^2} \tag{3-9}$$

Therefore, the following result is obtained for the method of Béchet and Kolb:

$$\frac{\Phi_{su}}{\Phi_{uu}} = \frac{C|G_{WFS}|^2|H_{atm}|^2\Phi_{e_1} + C|H_n|^2\Phi_{e_2}}{|C|^2|G_{WFS}|^2|H_{atm}|^2\Phi_{e_1} + |C|^2|H_n|^2\Phi_{e_2}} = \frac{C}{|C|^2} = \frac{C}{CC^*} = \frac{1}{C^*} \tag{3-10}$$

3-1-3 Conclusion for the method of Kolb and Béchet

Unfortunately, the clear conclusion is that Kolb and Béchet applied the spectral analysis method without realizing. As shown and proven above, this will lead to identification of the inverse controller. Since a good performing controller should look like the inverse of the plant, it is not surprising to think that the identified system is actually the plant itself. For comparison, the reader is referred to Figure 3-3. Indeed, the shape of the reconstructed estimate of the inverse controller looks, as should be expected, similar to the plant itself. This simulation was done with our own simulation system as explained in Appendix A without measurement noise to obtain the best possible result.

3-2 Parametric prediction error identification

Another approach for identifying the system in Figure 3-1 is the parametric prediction error identification method. The idea is that the true system $\mathcal{S}$ can be represented by a parametrized model structure $\mathcal{M} = \{G(q^{-1},\theta), H(q^{-1},\theta) \mid \theta \in \mathbb{R}^k\}$. When enough information about the characteristics of the plant and noise/disturbance $v(k)$ are available, it is possible to apply the parametric identification method. One should take notice that the information about the characteristics should be to the point that we are able to accurately parametrize the transfer function $H(q)$. So the true system $\mathcal{S}$ can be represented as follows:

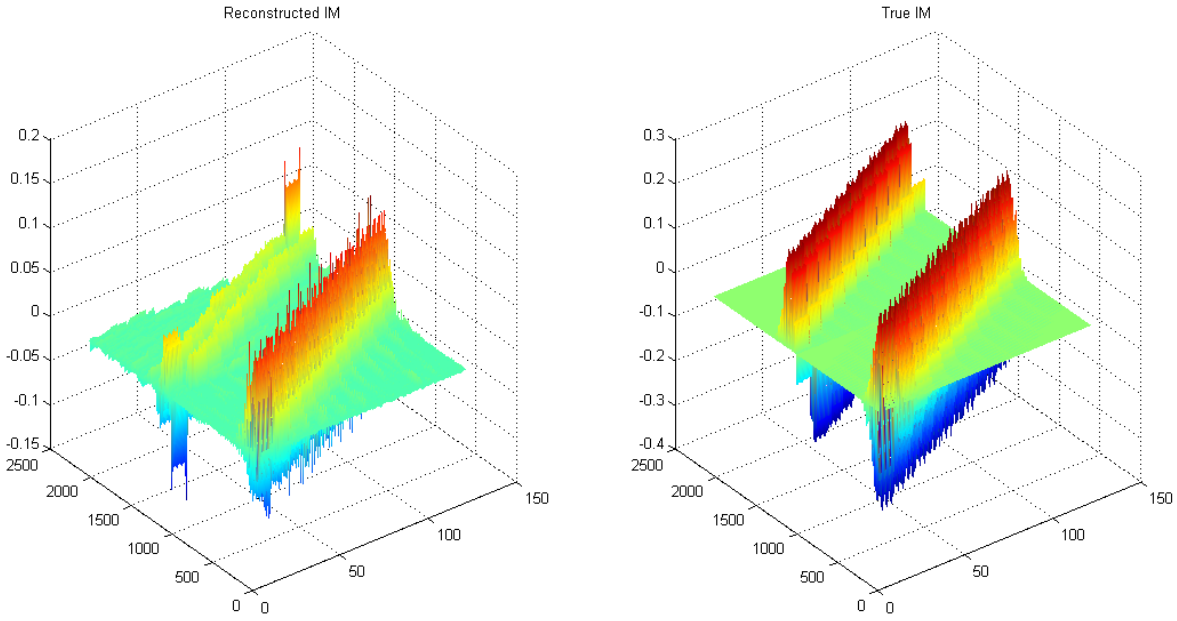

Figure 3-3: Reconstruction of the inverse controller obtained with the method described in [11] and [12]

$$y(k) = G(q^{-1})u(k) + v(k) \tag{3-11}$$
$$= G(q^{-1})u(k) + H(q^{-1})e(k) \tag{3-12}$$
$$= G(q^{-1}, \theta_0)u(k) + H(q^{-1}, \theta_0)e(k) \tag{3-13}$$

for some yet to be determined parameter θ_0. Mathematically this can be stated as $\mathcal{S} \in \mathcal{M}$. Now, we collect input-output data $Z^N = y(1), u(1), y(2), u(2), ..., y(N), u(N)$ from the true system. The idea is to determine for which parameter θ the input-output data of the model $[G(\theta), H(\theta)] \in \mathcal{M}$ matches best with the measured input-output data from the true system.

Before diving into the technical details of parametric identification in open-loop and closed-loop, we shall first define two important notions, namely identifiability and informativity. This will be followed by two sections devoted to parametric identification in open-loop and closed-loop respectively. After this, we shall discuss the necessary and sufficient requirements for informativity of an experiment. This Section, will be finalized by a discussion of the properties of parametric identification.

3-2-1 Open-loop parametric prediction error identification

As we have already explained the parametric method assumes that the true system $\mathcal{S}$ can be represented by a parametrized model structure $\mathcal{M} = \{G(q^{-1}, \theta), H(q^{-1}, \theta) \ |\theta \in \mathbb{R}^k\}$. So we can write the true system as follows:

$$y(k) = G(q^{-1})u(k) + H(q^{-1})e(k) = G(q^{-1}, \theta_0)u(k) + H(q^{-1}, \theta_0)e(k), \tag{3-14}$$

for some yet to be determined parameter vector θ_0.

After collection of data from the true system $Z^N = y(1), u(1), y(2), u(2), ..., y(N), u(N)$ from the true system, we will have to find for which parameter the data produced by the system matches best with the measured data from the true system. For this purpose, we first have to define the so called one-step ahead predictor. Let us start by manipulating the equation for the true system:

$$y(k) = G(q^{-1})u(k) + H(q^{-1})e(k) \tag{3-15}$$
$$= G(q^{-1})u(k) + [H(q^{-1}) - 1]e(k) + e(k) \tag{3-16}$$

substituting $e(k) = H(q^{-1})^{-1}[y(k) - G(q^{-1})u(k)]$ gives

$$y(k) = G(q^{-1})u(k) + [H(q^{-1}) - 1]H^{-1}(q^{-1})[y(k) - G(q^{-1})u(k)] + e(k) \tag{3-17}$$
$$= H^{-1}(q^{-1})G(q^{-1})u(k) + [1 - H^{-1}(q^{-1})]y(k) + e(k) \tag{3-18}$$

We should now notice that the expression $H(q^{-1})^{-1}G(q^{-1})u(k) + [1 - H(q^{-1})^{-1}]y(k)$ is fully determined by $G(q^{-1})$, $H(q^{-1})$ and by past observations $y(k-1)$ and $u(k-1)$ and differs only by $e(k)$ from $y(k)$. This expression is the so called one-step-ahead predictor of the given model [34]:

$$\hat{y}(k|k-1) = H^{-1}(q^{-1})G(q^{-1})u(k) + [1 - H^{-1}(q^{-1})]y(k) \tag{3-19}$$

Such a predictor can also be defined for the model set $\mathcal{M}$, which will be dependent on θ:

$$\hat{y}(k|k-1,\theta) = H^{-1}(q^{-1},\theta)G(q^{-1},\theta)u(k) + [1 - H^{-1}(q^{-1},\theta)]y(k) \tag{3-20}$$

The one-step-ahead prediction error is defined as:

$$\epsilon(k,\theta) = y(k) - \hat{y}(k|k-1,\theta) = H^{-1}(q^{-1},\theta)[y(k) - G(q^{-1},\theta)u(k)] \tag{3-21}$$

Now using the collected input-output data set Z^N, the true parameter θ_0 can be estimated using a quadratic criterion function on $\epsilon(k,\theta)$ by:

$$\hat{\theta} = arg\min_{\theta\in\mathbb{R}^k} V_N(\theta, Z^N) = arg\min_{\theta\in\mathbb{R}^k} \frac{1}{N}\sum_{k=1}^{N} \epsilon(k,\theta)^2 \tag{3-22}$$

If indeed $\mathcal{S} \in \mathcal{M}$, $G(q^{-1})$ strictly proper, $H(q^{-1})$ monic, stable and stably invertible then as $N \to \infty$, $\hat{\theta} \to \theta_0$ [34]. The properties of the covariance of $\hat{\theta}$ and $G(\hat{j\omega})$ will be discussed in depth in Section 3-2-4.

The quadratic criterion function $V_N = \epsilon(k,\theta)^2$ is the most frequently used. However, different generalizations are possible:

$$V_N(\theta, Z^N) = arg \min_{\theta \in \mathbb{R}^k} \frac{1}{N} \sum_{k=1}^{N} \epsilon(k,\theta)^2 \ell(L(q)\epsilon(k,\theta)), \tag{3-23}$$

where $\ell(\cdot)$ is a specific norm and $L(q)$ is some stable and linear filter. For more in depth information on the choice of $\ell(\cdot)$ and the effect of the filter $L(q)$ the reader is referred to Chapter 7 of [34]

3-2-2 Closed-loop parametric prediction error identification

Now, the theory for parametric identification in open-loop will be extended to closed-loop. For this, the setup in Figure 3-1b will be used.

If we define again the system $\mathcal{S} = [G(q^{-1}), H(q^{-1})]$ and define again a set of models that is able to represent the true system $\mathcal{M} = \{G(q^{-1},\theta), H(q^{-1},\theta) \mid \theta \in \mathbb{R}^k\}$ then an estimate can be obtained using the quadratic criterion function on $\epsilon(k,\theta)$:

$$\hat{\theta} = arg \min_{\theta \in \mathbb{R}^k} V_N(\theta, Z^N) = arg \min_{\theta \in \mathbb{R}^k} \frac{1}{N} \sum_{k=1}^{N} \epsilon(k,\theta)^2, \tag{3-24}$$

where ϵ is again given by:

$$\epsilon(k,\theta) = y(k) - \hat{y}(k|k-1,\theta) = H^{-1}(q^{-1},\theta)[y(k) - G(q^{-1},\theta)u(k)] \tag{3-25}$$

The application of the parametric identification approach on closed-loop systems has some important properties. Most notably, if the controller C is "sufficiently high order" in comparison with the complexity of the plant or if the controller C is nonlinear or time-variant, no explicit external excitation is needed for this method to work, i.e. the excitation coming from the noise or disturbance source can already be enough. More on this will be presented in Section 3-4.

3-2-3 Consistency problems when mismodeling the disturbance in closed-loop

In the previous Subsection, we have shown and proven that consistent estimates will be obtained for open-loop identification even if the disturbance is modeled incorrectly. The same path can be followed for closed-loop identification, this is shown and proven in Chapter 13.4 of [35].

When we follow the same road of derivation as shown above and after we fix the disturbance model to some $H_*(e^{j\omega}) \neq H_0(e^{j\omega})$, we arrive at the following final expression:

$$\hat{\theta} = arg \min_{\theta} \int_{-\pi}^{+\pi} \frac{|G_0(e^{j\omega}) + B(e^{j\omega}) + G(e^{j\omega},\theta)|^2 \Phi_u(\omega)}{|H_*(e^{j\omega})|^2} d\omega, \tag{3-26}$$

where $B(e^{j\omega})$ is given as:

$$B(e^{j\omega}) = \frac{C_0(e^{j\omega})H_0(e^{j\omega})}{1 + C_0(e^{j\omega})G_0(e^{j\omega})}(H_0(e^{j\omega}) - H_*(e^{j\omega}))\frac{\sigma_e^2}{\Phi_u} \tag{3-27}$$

.

We can already see that the estimate converges to the value of $\hat{\theta}$ for which $\hat{G}(e^{j\omega}, \hat{\theta}) = G_0(e^{j\omega}) + B(e^{j\omega})$, which means that as long as there is a mismatch in the modeling of the disturbance H, i.e. $H \notin \mathcal{H}$, there will be a bias in the estimate $\hat{G}(e^{j\omega}, \hat{\theta})$ in the form as described above.

In literature, there are several possibilities to lower or even to completely get rid of the bias [36].

3-2-4 Stochastic properties parametric identification

The parametric prediction error identification method is asymptotically unbiased. One can also understand that the parametric method will have lower variance in comparison with the spectral method, simply because it takes more information about the system into account.

Let $\hat{\theta}_N$ be the identified parameter vector for θ_0. It will be a stochastic variable that is asymptotically normally distributed as [35]:

$$\hat{\theta}_N \sim \mathcal{N}(\theta_0, P_\theta), \tag{3-28}$$

where P_θ is the so called covariance matrix, which is defined as [35]:

$$P_\theta = \frac{\sigma_e}{N}(E(\phi(t, \theta_0)\phi(t, \theta_0)^T))^{-1}, \tag{3-29}$$

where σ_e is the variance of the gaussian white noise and ϕ is defined as:

$$\phi(t, \theta) = -\frac{\partial \epsilon(t, \theta)}{\partial \theta} = \frac{\partial \hat{y}(t, \theta)}{\partial \theta} \tag{3-30}$$

The inverse of the covariance matrix is the so called information matrix, which needs to be positive definite for a successful identification. More on necessary and sufficient conditions to achieve a successful prediction error identification will be explained in Sections 3-3 and 3-4.

Also the estimated plant $\hat{G}$ is an asymptotically normally distributed random variable. A common method to go from the covariance matrix P_θ, which represents the covariance of the parameters, to the covariance of the transfer function is to use a first order Taylor series expansion [37]. Then the transfer function covariance is defined as follows:

$$cov(\hat{G}(j\omega, \hat{\theta}_N)) = E[(G(e^{j\omega}, \hat{\theta}_N) - G(e^{j\omega}, \theta_0))^2] \tag{3-31}$$

$$= T(e^{j\omega}, \theta_0)P_\theta T(e^{j\omega}, \theta_0)^T \tag{3-32}$$

with $T(z, \theta)$ given as:

$$T(z,\theta) \triangleq \begin{bmatrix} Re(\nabla_G^T(z,\theta)) \\ Re(\nabla_G^T(z,\theta)) \end{bmatrix} \tag{3-33}$$

$$\nabla_G(z,\theta) = \frac{\partial G(z,\theta)}{\partial \theta} \tag{3-34}$$

The following first order approximation was used in obtaining this estimate:

$$G(z,\theta_0) \approx G(z,\hat{\theta}_N) + \nabla_G^T(z,\theta_0)(\theta_0 - \hat{\theta}_N) \tag{3-35}$$

An important advantage of parametric prediction error identification over the spectral method is that it can "turn" part of the disturbance and/or noise into useful information in closed-loop.

3-3 Notions of identifiability and informativity for prediction error identification

The notions of identifiability and informativity and therewith input signal design are an important aspect in system identification. In Appendix B, we shall introduce and formally define the notions of identifiability and informativity.

3-4 Necessary and sufficient conditions for a unique minimum of the prediction error criterion

Earlier, we have defined the notions of identifiability and informativity. These are the two ingredients necessary to achieve a successful prediction error identification experiment. Only when the combination of these two requirements are met, the quadratic criterion function as defined in Equation 3-22 will have a unique minimum. This is equivalent to saying that the information matrix, the inverse of the covariance matrix as defined in Equation 3-29, is positive definite.

We will first start by discussing the necessary and sufficient conditions for the open-loop case, because in order to understand the requirements for closed-loop, we shall first analyze the requirements for informativity in open-loop. After this, we will continue with closed-loop.

3-4-1 Conditions in open-loop

Assume that the true system $\mathcal{S} \in \mathcal{M}$, where $\mathcal{M} = \{G(q^{-1},\theta), H(q^{-1},\theta)\}, \theta \in \mathbb{R}^k$, such that $G(q^{-1},\theta)$ are rational functions:

$$G(q^{-1},\theta) = \frac{B(q^{-1},\theta)}{F(q^{-1},\theta)} = \frac{-q^{-n_k}(b_1 + b_2 q^{-1} + ... + b_{n_b} q^{-n_b+1})}{1 + f_1 q^{-1} + ... + f_{n_f} q^{-n_f}} \tag{3-36}$$

Then an input sequence that is persistently exciting of order n_b+n_f is sufficiently informative with respect to $\mathcal{M}$. If furthermore, the conditions for identifiability are met, i.e. the model structure is chosen such that the true system is represented by a single unique model, the information matrix will be positive definite [34].

3-4-2 Conditions in closed-loop

The presence of the feedback in the structure of the problem make the conditions for identifiability in closed-loop more involved. This is for the reason that, not only there are requirements on the model set now, but also requirements on the structure of the problem. Let us now try to understand this problem better by means of the following autonomous first order system with a proportional controller:

$$\begin{aligned} y(k) + ay(k-1) &= bu(k-1) + e(k) \\ u(k) &= fy(k) \end{aligned} \tag{3-37}$$

Rewriting results in the following autonomous system:

$$y(k) + (a - bf)y(k-1) = e(k) \tag{3-38}$$

Although all the conditions as mentioned in the previous Subsection for open-loop are met and although the input $u(k)$ is persistently exciting since it consists of filtered white noise, we can see in this example that it is impossible to identify the parameters a and b even if we know f, because all $\hat{a}, \hat{b}$ with $\hat{a} = a+\gamma f$ and $\hat{b} = b+\gamma$, where γ is any arbitrary scalar, satisfy the same system description.

Notice that the above described problem would not have appeared if the controller was time-variant or nonlinear. In that case, the requirements for identifiability are met and, thus, identification is possible as soon as the command $u(k)$ is persistently exciting. To obtain better insight into this problem and how it arises, we will have to look back at Equation B-8:

$$\overline{E}[\Delta W_u(q)u(k) + \Delta W_y(q)y(k)]^2 = 0 \tag{3-39}$$

Now, suppose that there are two different models W_1 and W_2 in the model set for which this equation holds without implying that $W_1 = W_2$ as shown in the example above. So the expression above can indeed be zero while $\Delta W_u(q) \neq 0$ $\Delta W_u(q) \neq 0$. Let us ask which precondition is required for such an equality to hold. One can understand by some insight that this is only possible if there exist some linear and time-invariant relationship between the input $u(k)$ and output $y(k)$

$$\Delta W_u(q)u(k) \sim -\Delta W_y(q)y(k) \tag{3-40}$$

From this, we can already understand why identifiability is guaranteed for the cases where the controller C is time-variant or nonlinear if $u(k)$ is persistently exciting. It should be mentioned that time-variance of the controller can also be reached by switching between different settings for the controller during the experiment.

So, for the situation in which such a linear and time-invariant relationship holds, the conditions for identifiability and informativity become more involved. **In those cases, if the controller is "more complex" than the plant then identifiability is guaranteed and thus informativity is guaranteed when the noise or disturbance signal is sufficiently exciting.**

Now we will formalize these conditions regarding complexity for the Box-Jenkins model structure, which we will be using in the application of our research. Let us consider the class of model structures $\mathcal{M} = \{G(z,\theta), H(z,\theta) \,|\theta \in \mathbb{R}^k\}$ where $G(z,\theta)$ and $H(z,\theta)$ are given according to the Box-Jenkins parametrization structure:

$$G(z,\theta) = \frac{z^{-n_k} B(z,\theta)}{F(z,\theta)}, \tag{3-41}$$

$$H(z,\theta) = \frac{L(z,\theta)}{D(z,\theta)}, \tag{3-42}$$

with $B(z,\theta)$, $L(z,\theta)$, $D(z,\theta)$ and $F(z,\theta)$ are polynomials of degree n_b, n_l, n_d, n_f respectively. The controller is given by $C_{cntrl}(z) = \frac{X(z)}{Y(z)}$, with $X(z)$ and $Y(z)$ polynomials of degree n_x and n_y respectively.

Furthermore, we will make multiple assumptions regarding the system. First of all, there are no terms that cancel out in the polynomial set $B(z,\theta)$ and $L(z,\theta)$. The polynomial set $D(z,\theta)$ and $L(z,\theta)$ are assumed to be coprime and the same will hold for the polynomial set $X(z)$ and $Y(z)$ as well. The closed-loop denominator polynomial does not cancel out any root in $L(z,\theta)$. Finally, the degrees n_k, n_b, n_l, n_f and n_d are assumed to be known in advance.

Then only if and only if either $n_x + n_k > n_d + n_f$ or $n_y > n_b + n_d$ the information matrix is positive definite or, in other words, the quadratic criterion function $V = \epsilon^2(t,\theta)$ as defined in equation 3-22 has a unique global minimum at θ_0 [38] [39].

3-5 Novel least cost experiment design paradigm for parametric identification by Gevers and Bombois

Classically, optimal experiment design was all about maximizing the accuracy of the identified system by optimizing the power spectrum of the input signal, possibly under certain predefined constraints on time and/or on the input signal. This is very useful for systems that need identification once and afterwards can continue their operation. In those cases, it makes sense to focus on obtaining an accurate model since it will be done once only.

This is, however, not of much use for our application in which we will need to calibrate the IM of the telescope regularly. As explained in Section 1-2, we need a method that disturbs the closed-loop operation of the telescope as low as possible while guaranteeing a certain identification accuracy. So in our case, there will be an important trade-off between achievable accuracy for the experiment and the impact of it on the closed-loop operation of the telescope. Therefore, it makes more sense to apply a method which takes into account the cost of an experiment in terms of perturbation of the closed-loop operation and duration or a combination of both. Such a paradigm was proposed for the first time in [40].

To explain how the method works, we have to go back to the variance of the identified plant as derived in the previous Section in Equation 3-31. Since the variance of the identified plant measures how far the identified plants will be spread out from the true plant, we need to define boundaries on the modeling error in terms of requirements on the expression for the variance:

$$r_u(\omega) = \alpha\sqrt{cov(\hat{G}(j\omega, \hat{\theta}_0))} \tag{3-43}$$

$$= \alpha\sqrt{\lambda_1(T(e^{j\omega}, \theta_0)P_\theta T(e^{j\omega}, \theta_0)^T)} \tag{3-44}$$

Clearly, it is not possible to guarantee with 100% certainty that the modeling error of the identified plant will be within a certain boundary. This is only possible with a certain probability level and that is where the constant α comes into picture. If we would want $Pr(|\hat{G} - G_0| < r_u) > 0.95\%$, the constant α is chosen in such a way that $Pr(\chi^2(n) < \alpha^2) > 0.95$, where n is the number of unknown variables in the parametrized model of $G(z, \theta)$.

As mentioned earlier, an important aspect of the paradigm in [40] is the definition of the cost for identification. Different costs were defined for open-loop and closed-loop. In open-loop, it is possible to limit yourself just to the power content of the external excitation signal $r(t)$ which is used for identification. In closed-loop, however, this is not such an obvious choice anymore. Therefore, an alternative definition for the cost of an identification experiment was chosen, which is more appropriate for the nature of the actual cost. To understand this, we have to look back at Figure 3-1b and try to understand the difference between normal operation of the closed-loop setup and operation of the closed-loop setup while being identified. In this case, we will make a derivation only for the signal r_2. A similar derivation for r_1 is straightforward and will thus not be covered. The plant input u and the output y under normal operation are given as:

$$u = \frac{-C}{1+GC} \quad v \tag{3-45}$$

$$y = \frac{1}{1+GC} \quad v \tag{3-46}$$

Clearly, the disturbance signal v is the single source of excitation under normal operation. During an identification experiment, however, we will use the signal r_2 to excite the system to obtain information about the plant. Thereby, we are also interrupting normal operation, since we are now introducing another output term due to our excitation signal r_2:

$$u = \frac{1}{1+GC} \quad r_2 \quad + \quad \frac{-C}{1+GC} \quad v \quad = \quad u_{r_2} \quad + \quad \frac{-C}{1+GC} \quad v \tag{3-47}$$

$$y = \frac{G}{1+GC} \quad r_2 \quad + \quad \frac{1}{1+GC} \quad v \quad = \quad y_{r_2} \quad + \quad \frac{1}{1+GC} \quad v \tag{3-48}$$

Above, we have introduced the terms u_{r_2} and y_{r_2}, which should be interpreted as plant input due to r_2 and output due to r_2 respectively. These two terms are the "interruptions", or in

other words "the cost", that we introduced for the purpose of identification, because due to these terms the imaging quality of the telescope will deteriorate. Now, it is also possible to measure the cost in terms of the spectra corresponding to u_{r_2} and y_{r_2}:

$$\mathcal{J}_{r_2} = \beta_u \left(\frac{1}{2\pi} \int_{-\pi}^{+\pi} \Phi_{u_{r_2}}(\omega) d\omega \right) + \beta_y \left(\frac{1}{2\pi} \int_{-\pi}^{+\pi} \Phi_{y_{r_2}}(\omega) d\omega \right), \tag{3-49}$$

where β_u and β_y are weights that can be adjusted according to what is important for the closed-loop operation.

The cost $\mathcal{J}_{r_2}$ can also be expressed in terms of the spectrum of r_2:

$$\mathcal{J}_{r_2} = \beta_u \left(\frac{1}{2\pi} \int_{-\pi}^{+\pi} \frac{1}{|1+GC|^2} \Phi_{r_2}(\omega) d\omega \right) + \beta_y \left(\frac{1}{2\pi} \int_{-\pi}^{+\pi} \frac{|G|^2}{|1+GC|^2} \Phi_{r_2}(\omega) d\omega \right) \tag{3-50}$$

The derivation of the expression for the cost function for an excitation signal at r_1 is straightforward and follows the same procedure as above.

For our research purposes, in order to obtain insight in the workings of the least cost identification method applied to AO systems, we will initially define the cost purely as the input cost, which is the usual way to define the cost in open-loop:

$$\mathcal{J}_{r_{1,2}} = \frac{1}{2\pi} \int_{-\pi}^{+\pi} \Phi_{r_{1,2}}(\omega) d\omega \tag{3-51}$$

The idea is now that we will choose the optimal trade-off between experiment duration and spectrum richness on the one hand and obtained accuracy on the other hand. Prior to the experiment the maximum allowed error r_{adm} will be known already depending on the identification objective. If we also fix the experiment duration N, we can obtain an affine optimization problem in the spectrum Φ_r:

$$\min_{\Phi_r} \quad \mathcal{J}_r \qquad s.t. \quad \alpha \sqrt{cov(\hat{G}(j\omega, \theta_0)} < r_{adm} \tag{3-52}$$

$$\min_{\Phi_r} \quad \mathcal{J}_r \qquad s.t. \quad \alpha \sqrt{\lambda_1 (T(e^{j\omega}, \theta_0) P_\theta T(e^{j\omega}, \theta_0)^T)} < r_{adm} \tag{3-53}$$

For our application both the experiment duration and spectrum are of importance. Therefore, it is not possible to fix either one of the parameters in order to obtain an affine problem. Instead, we will determine the optimal spectra Φ_r for a number of experiment durations. Thereby, we can create a "trade-off graph" where the cost is depicted versus the duration of the experiment. Clearly, for increasing experiment duration N the cost function $\mathcal{J}_r$ decreases. This allows us to find the "optimal" combination for the duration of the identification and the induced interruption $\mathcal{J}_r$.

3-5-1 Important drawback of the least-cost identification paradigm

A key problem in the least-cost identification paradigm is that the covariance matrix in the optimization problem shown in Equation 3-52 not only depends on the spectrum of the excitation signal and admissible error. The depends on the true system $G(z, \theta_0)$, and therewith also on the true parameter vector θ_0, but also on the true disturbance or noise variance σ_e^2. This is basically a chicken-and-egg problem, because the optimal experiment basically depends on what it should actually estimate [41].

This is, however, inherent to every optimal experiment design method. A standard method to solve for this issue is to replace the true parameter vector θ_0 by an initial estimate $\hat{\theta}_{init}$ and σ_{init}^2:

$$\min_{\Phi_r} \quad \mathcal{J}_r \qquad s.t. \quad \alpha\sqrt{\lambda_1(T(e^{j\omega}, \hat{\theta}_{init})P_\theta T(e^{j\omega}, \hat{\theta}_{init})^T)} < r_{adm} \tag{3-54}$$

These estimates can be obtained by means of a simple spectral identification experiment.

For classic optimal experiment design, where the objective was to obtain maximal accuracy without considering the cost, this solution served very well, because the objective of maximal accuracy practically ensured robustness of the identification experiment. However, in this case, we are dealing with a least-cost paradigm, where we would only want to guarantee the necessary accuracy instead of the maximum accuracy. This can cause problems with convergence. Therefore, in the following, we either have to provide a solution for this problem or make certain assumptions regarding our knowledge of the plant.

Chapter 4

Research proposal for least cost closed-loop identification of the interaction matrix of an AO system

This Chapter will focus on different types of approaches to identify the IM in closed-loop with as low as possible additional interruptions caused by the excitation signal. The different candidate methods from the previous Chapter will be discussed one by one. While doing this we will refer to Figure 4-1 regularly.

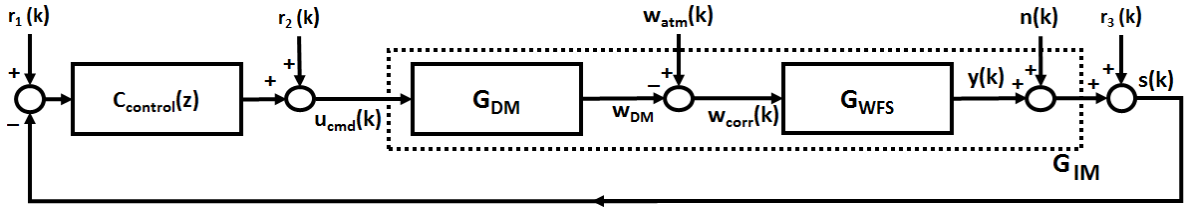

Figure 4-1: Closed-loop identification setup for the telescope

Our initial discussion will regard the **supposedly** costless method proposed by Kolb and Béchet in [11] and [12] and explain why this idea is **fundamentally wrong**. While doing this, we will frequently refer back to our derivations and proves in Section 3-1.

From here, we will make the switch to parametric prediction error identification and explain how it can be applied to our system. The model set selection is an important task for parametric prediction error identification, so we will devote a separate subsection on this.

This will be followed by a separate Section dedicated to how we might apply costless parametric prediction error identification to our problem. In Section 3-4-2, we have already seen that in some cases the excitation coming from the disturbance or noise, which is fed back into the system by the controller can be sufficient for identification purposes. It would be very interesting for our situation if we could identify the IM using the disturbance coming from

the atmospheric turbulence. We will show that costless identification works perfectly on a SISO AO system when accurate information about the noise or disturbance characteristics are present and the requirements as explained in Section 3-4-2 are met. In our example, we will assume perfect knowledge about the disturbance characteristics. Therefore, this will be a demonstration of the principle by showing how to apply true costless identification on a SISO AO system.

Finally, we will discuss on how the paradigm proposed by Michel Gevers can aid us in designing the optimal input for our application when we decide to apply parametric prediction error identification. We will discuss what kind of bottlenecks we can expect and in what way we will try to deal with these.

The chapter will be closed by a final consideration and conclusion which will contain our research proposal for least cost closed-loop identification. We will discuss which method we foresee as the best option and why. This discussion will of course include a deliberation on the positive sides and possible bottlenecks of the method.

4-1 Supposedly costless closed-loop identification proposed by Kolb and Béchet

The method proposed by Kolb and Béchet has been extensively discussed in Section 3-1. We have clearly shown and proven that they are actually simply applying the open-loop spectral identification method after prefiltering, without any explicit external excitation. We have also shown and proven that this results in the identification of the static gain of the inverse controller. Furthermore, we have also tackled the fundamental assumption of Kolb and Béchet in [11] and [12], which is that the correlation between the disturbance and plant input can disappear by prefiltering the data. This has been mathematically proven at the end of Section 3-1 in terms of the autocorrelation of the disturbance.

The confusion regarding the results are, however, understandable. In Figure 3-3, we have shown that the reconstructed inverse controller resembles the true static IM matrix. Therefore, although their very first assumption is fundamentally wrong, Kolb and Béchet were probably not able to recognize their mistake from the results.

4-2 Parametric prediction error identification

By using an external excitation signal to either r_1 or r_2 it is possible to apply parametric prediction error identification in closed-loop to the AO system as shown in Figure 4-1. The theory on how to do this has been extensively explained in Section 3-2-2 and, therefore, we will not devote a repetition of the existing knowledge in this Section. Instead, we will

4-2-1 Model set selection

The choice of our model set will be an important and fundamental decision in the process of parametric prediction error identification. First of all, we need to choose an appropriate

model structure. Followed by our choice for the model orders. The final task is on how to parametrize the chosen models.

In our case, we are searching for a static representation of the IM, the open-loop plant. Furthermore, we know that the disturbance that we are dealing with is highly complex and thus it is advisory to model it separately from the open-loop plant, since we need all the possible freedom. The choice for the model structure Box-Jenkins is in that case already a straightforward choice. The model order for the open-loop plant G_{IM} is also clear, which will be model order 1 since it is static. In SISO $G_{IM}(q,\theta) = \theta$. For a MIMO system this would be a matrix representation of the same form.

The model order and model parametrization for the disturbance is not that straightforward. As depicted in Figure 2-6, the Von Karman spectrum of atmospheric turbulence has a fractional slope, which has to be represented by a polynomial, i.e. a rational function. Weierstrass has proven that any continuous function, and thus also fractional function, can be estimated by a polynomial [42]. The choice for the polynomial degree determines how close the estimation will become. In our case, we need to beware not to give too much freedom in the model for H, since this will allow for overfitting. Therefore, the modeling of the disturbance and choosing an appropriate parametrization will be an important part of our research. Especially because in closed-loop consistency is lost when $H \notin \mathcal{H}$. This will be explained in the following Subsections.

There is a systematic method to choose an appropriate model order. The idea is to evaluate and compare the value of the criterion function $V_N(\hat{\theta}_N, Z^N)$ for different model orders. Until we have reached the appropriate model order we should expect to see substantial decrease in the final value of the criterion function $V_N(\hat{\theta}_N, Z^N)$. Although it will continue to decrease little by little, once the appropriate order is reached, we expect to see saturation in the decrease. The continuation of the decrease does not mean that the model is a better representation of the true system, because the extra freedom provided in our model will simply be used to adjust better to our specific data set, which means that it will adjust itself according to the noise sequence. This can also be understood when one validates the obtained estimate with a separate data set, because, although in the first data set a higher model order delivered a better fit, this will be untrue when applied to a validation with a separate data set. This method is called cross-validation. Therefore, one should also realize that there is a drawback in choosing a higher model order. Furthermore, the added complexity might also result in optimization problems, because we might get stuck in a local minimum easier when the complexity of the applied model increases.

4-3 Costless parametric prediction error identification: prove of principle

After the Section regarding the erroneous method proposed by Kolb and Béchet, one might ask whether costless closed-loop identification of the IM is possible without explicit external excitation. The simple answer to the addressed question addressed is of course yes. The theoretical background and prove on this has been discussed extensively in Section 3-2-2. In this Section, we will demonstrate how to apply costless identification, i.e. identification

without explicit external excitation, on a SISO AO system in order to successfully identify the static IM in closed-loop.

The more comprehensive answer to the addressed question is, of course, not this straightforward. For such a method to be successful, one should at least be able to parametrize the disturbance accurately. Otherwise, this will lead to biases in the identification, which will be characterized mathematically in Section 3-2-3. Additionally, the modeling of atmospheric turbulence is highly complex and still an involved topic today. Turbulence is highly non-linear and time-variant, which complicates the problem. Thus, one should also consider the time-variant characteristics with respect to the identification duration. An important question to address would be how long an identification experiment is allowed to take before the time-variant characteristics become too dominant to obtain accurate identification.

We will now apply closed-loop identification on a simplified AO system without external excitation following the theory described in Section 4-2. The setup is shown in Figure 4-2. Instead of a MIMO gain, a SISO gain is chosen. The feedback controller is again a pure integrator. The disturbance, which should represent the atmospheric turbulence, is also simplified to a signal $w_{atm}(k)$ which is obtained by filtering zero mean Gaussian white noise with a variance of 1 with the following filter:

$$H(q^{-1}) = \frac{1}{1 - 0.5q^{-1}} \tag{4-1}$$

For this example, we assume that the disturbance model is exactly known as described above. Therefore, the single parameter to be determined will be the SISO gain, which equals 9 in this case. The noise $e(k)$ is pure white noise with a variance that equals 1.0% of the variance of the output without noise, which is a realistic value for true AO systems. We will regard the measurement noise equal to zero, since it is negligible relative to the total signal.

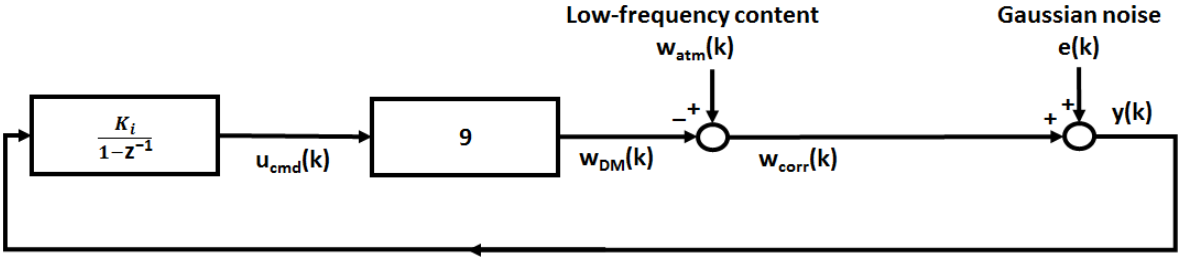

Figure 4-2: Closed-loop setup of the SISO AO system for demonstration of costless identification

Now, we have to define the one-step-ahead prediction error:

$$\epsilon(k,\theta) = H^{-1}(q^{-1},\theta)[y(k) - G(q^{-1},\theta)u(k)] \tag{4-2}$$
$$= (1 - 0.5q^{-1})[y(k) - \theta u(k)] \tag{4-3}$$
$$= y(k) - \theta u(k) - 0.5y(k-1) + 0.5\theta u(k) \tag{4-4}$$

The quadratic criterion function is a function of the one-step-ahead predictor and will look like:

$$V_N(\theta) = \frac{1}{N}\sum_{k=1}^{N}\epsilon(k,\theta)^2 = \frac{1}{N}\sum_{k=1}^{N}[y(k) - \theta u(k) - 0.5y(k-1) + 0.5\theta u(k)]^2 \tag{4-5}$$

Application of the quadratic criterion function described as above leads to Figure 4-3. The parameter θ has been successfully identified for our simplified AO system by being $\theta = 9.0$.

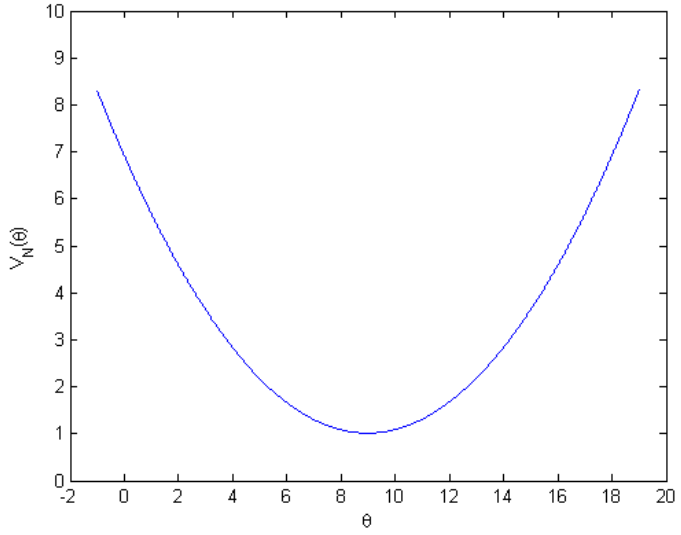

Figure 4-3: Plot of the quadratic criterion function for the simplified AO system

Now, we have demonstrated the principle of costless identification using an example of a simplified AO system which was identified using just the excitation coming from the disturbance. So it is possible to identify the AO system without explicit external excitation, but we do need to be able to capture the dynamics of the disturbance into a parametrized model. As soon as we fail to do this, consistency problems as described in Section 3-2-3 will occur.

In Section 5-5, we will discuss more in depth in which cases costless closed-loop identification is possible, this time specifically for our AO system. In the same Section, we will discuss that in those cases where identifiability is given, theoretically, unlimited accuracy is possible as experiment duration tends to infinity. Finally, also in Section 5-5, we will prove that H has completely no influence on the amount of information provided in closed-loop.

4-4 Least cost experiment design paradigm proposed by Gevers and Bombois

As explained earlier, it is important for us to identify the IM with a predetermined accuracy while keeping the deterioration of the closed-loop process as low as possible. In closed-loop, we have multiple possibilities for excitation locations and in closed-loop the excitation signal might also get rejected by the controller partially or completely. This makes it much more involved to determine a ”good” excitation signal for identification purposes. Therefore, it is necessary to have a systematic approach to this problem in which we can exactly quantify

our desires in terms of experiment cost and accuracy. Therefore, the choice for the paradigm of Gevers and Bombois seems straightforward. There are, however, a few issues needed to overcome before being able to apply this method for our research purposes.

There is first of all an important drawback of the least cost paradigm, which is the paradox as we have explained earlier in Section 3-5-1: the optimal experiment depends on the system which is to be estimated by the optimal experiment. A proposed solution is to design the optimal experiment based on an estimate obtained from a short and simple initial experiment [43]. Let us now imagine that this experiment is either too short or too simple in the sense that we obtain a bad estimate which causes the designed "optimal experiment" not to be optimal at all. This means that we cannot possibly achieve the desired accuracy. In Section 3.1 [43], this issue is shortly touched upon, but no further solutions are provided.

As for our current research purposes, we will in first instance assume "perfect" knowledge of the plant. Later on, in Chapter 7, specifically in Section 7-1, we will have an in depth discussion on the shortcomings of this assumption and provide a solution to robustify our least cost experiment design procedure.

We can also notice two important issues with the constraints as formulated in Equation 3-52. First of all, there are an infinite number of constraints, which means that the optimization problem as it currently stands is practically impossible to solve. The last important issue is that in the current form of Equation 3-52, we will not be able to apply LMI solvers, since the constraints are not affine in the decision variable $\Phi_r(\omega)$. In Section, 5-4, we will see that we can easily sample the constraints in order to obtain a finite dimensional problem. Also, a more elaborate solution, using the KYP lemma will be explained. Finally, the Schur complements will be used to linearize the constraints as given in Equation 3-52.

Lastly, there is a problem with the decision variable $\Phi_r(\omega)$ itself, which is its infinite dimensionality. This problem can be solved by parametrizing $\Phi_r(\omega)$. In Section 5-3, we will discuss different methods to parametrize our decision variable and show that a multisine parametrization is better than the FIR parametrization applied in [43]. Later on, in our evaluation in Section 7-2, we will revisit this consideration, this time taking criteria for robustness and MIMO into mind as well.

4-5 Final choice identification methods

Let us address our conclusion regarding the different methods in the same sequence as we have ordered them in this Chapter.

It should be clear by now that spectral identification can indeed estimate the open-loop plant at any desired accuracy. However, since no model for the disturbance is taken into account, the cost for arriving at a desired accuracy will always be higher in comparison with other more advanced identification techniques. For this reason, the spectral identification method can solely serve as a tool for identification to obtain an initial estimate of the design to serve as a basis for the experiment that we have to design.

Clearly, the method of Béchet and Kolb identifies the inverse controller and is, thus, next to being fundamentally wrong, of no use at all. We can be short about this.

We have shown that as long as $H \in \mathcal{H}$, the parametric prediction error identification works well in closed-loop. Therefore, accurate and correct modeling of the disturbance H is of extra importance. In closed-loop, a bias will emerge as soon as $H \notin \mathcal{H}$. These consistency problems that will emerge were discussed and explained in Section 3-2-3. In the following, each time we will assume, "perfect" knowledge of the disturbance characteristics H.

In Section 4-3, we have shown that costless identification is possible by providing a simplified example, which assumed "perfect" knowledge of the disturbance characteristics H. Practically, we already know that "perfect" modeling is impossible and even good modeling might be cumbersome since atmospheric turbulence is highly complex, nonlinear, and time-variant.

Although there are certain question marks regarding costless identification, in the following Chapter, we will dive deeper into costless identification, because it does have great potential if we are able to accurately model and capture the disturbance characteristics.

Finally, we have discussed how the paradigm as proposed by Gevers and Bombois can aid us in our optimal experiment design. We are looking for an experiment that achieves a prespecified accuracy at the lowest possible cost and this is exactly what the novel paradigm is about.

Therefore, in the following Chapter, we shall focus our attention on the open-loop and closed-loop identification of three different AO systems with the least cost identification paradigm. The three different systems taken into consideration will be a unit-delay gain, a second order system with only the gain as a variable, and finally a second order system with full freedom, i.e. three free variables.

Both in open-loop and closed-loop, the cost will be defined as the total energy of the excitation spectrum. Thus, initially, when only the total energy of the excitation spectrum is considered, the imposed optimization problem for the reference signals r_1 or r_2 will become as follows:

$$\min_{\Phi_{r_{1,2}}} \frac{1}{2\pi} \int_{-\pi}^{+\pi} \Phi_{r_{1,2}}(\omega) d\omega \quad s.t. \quad \alpha \sqrt{\lambda_1(T(e^{j\omega}, \theta) P_\theta T(e^{j\omega}, \theta)^T)} < r_{adm} \tag{4-6}$$

Finally, we will consider the deterioration of the ordinary closed-loop operation as being the cost, which is clearly more interesting for our research purposes. While the constraints of the optimization problem stay exactly the same the costs for the two imposed optimization problems related to the reference signals r_1 and r_2 will respectively become:

$$\begin{aligned} \mathcal{J}_{r_1} &= \frac{1}{2\pi} \int_{-\pi}^{+\pi} \frac{|GC|^2}{|1+GC|^2} \Phi_{r_1}(\omega) d\omega \\ \mathcal{J}_{r_2} &= \frac{1}{2\pi} \int_{-\pi}^{+\pi} \frac{|G|^2}{|1+GC|^2} \Phi_{r_2}(\omega) d\omega \end{aligned} \tag{4-7}$$

There are, however, just like with every method some issues that we need to be overcome to apply the method to our problem. First of all, we can notice that in the above equations the optimal experiment is naturally based on knowledge of the true system. Since this is not available yet, designing the true optimal experiment is impossible and, therefore, we have to rely on initial estimates for designing the optimal experiment. Although this brings along robustness issues on its turn, we will assume our knowledge of the different plants to be perfect.

Later on, we will also look into possible robustness issues when we consider the stochastic character of these estimates. For example, what happens when the initial estimate is too poor to result in a good experiment. Naturally, you cannot achieve a good identification of the underlying system without a "good" experiment, and we also cannot reach a good experiment without a good initial estimate. However, the question is now of course how good does the initial estimate have to be to guarantee a certain accuracy in the experiment design or how can we cope with the uncertainty present in the initial estimate. In Section 7-1, we will deal with this issue and formulate a solution to robustify the experiment design procedure.

We also mentioned two problems regarding the constraints. First of all, the constraints are currently not expressed in terms of the optimization variable. Most importantly, however, we need to ensure that we arrive at a description which is affine in terms of the optimization variables. This will be discussed and solved in Section 5-4.

Finally, we also need to use a finite dimensional parametrization for the infinite dimensional $\Phi_r(\omega)$. This will be considered in depth in Section 5-3.

Chapter 5

Application of least cost identification

In the previous Chapter, we ended with the conclusion that it is best to apply the newly developed least cost identification paradigm to our problem at hand. In this Chapter, we will present the issues that we came across. The applied solutions and results will be presented for each issue.

Our first Section will be devoted to the initial assumptions that we made in our research.

Consequently, in Section 5-2 we will discuss which excitation location is best to use for the purpose of closed-loop identification and which one would be more efficient in terms of cost. This has not been considered in [43] or earlier literature.

In succession, we will look into different methods of parametrizing our infinite dimensional input power spectrum in Section 5-3. An FIR parametrization was proposed and applied in [43]. However, we suggest that a sinusoidal parametrization is more efficient both in terms of cost and computational load.

This will be followed by a short summary of the literature on how to obtain a convex formulation of the optimization in Section 5-4.

From there on, we will dwell deeper into costless closed-loop identification in Section 5-5. In the previous Chapter, we had already shortly touched upon this topic. In this Section, we will continue this discussion by explaining when exactly costless identification is applicable specifically in the case of a Box-Jenkins model. After this, we will derive exact expressions for the information matrix in case of costless identification. Also, by further working out the expressions for the information matrix, we will prove that neither the shape nor the total energy of the disturbance spectrum effects the accuracy of the experiment.

An important part of our research we have spent on overcoming numerical issues. Therefore, finally, in Section 5-6, we will discuss these issues and provide solutions for them.

5-1 Initial assumptions

Before starting to apply the least cost identification paradigm developed by Bombois and Gevers, we will first make initial assumptions in advance. In Figure 4-1, we can still see the measurement noise is depicted as being n. Since the measurement noise is already engineered to be very small, i.e. negligible in AO systems [13], we have decided to assume $n = 0$. Hereby, with negligible loss of accuracy, we will have significantly reduced the complexity of our problem by making this assumption.

A second important assumption is that we will assume the systems that we will look into to be exact. So each time, we will try to find the least cost excitation spectrum for a hypothetically perfectly known system. This means that, in first instance, we will not take into account issues such as estimate accuracy and robustness of the least cost identification procedure.

The same will also hold for the modeling of the disturbance H.

Finally, our analyses will be restricted to the SISO case only.

Later, in Chapter 7, we will get back to the assumption of "perfect" knowledge, and we will also provide a method to robustify our least cost experiment design procedure. We will also revisit the assumption on the accuracy of the modeling of H and provide several suggestions for future work. Finally, although MIMO considerations have been left out in our research, we will spend time to also evaluate how we might extend our method to this situation which require different criteria.

5-2 Which excitation location to use for closed-loop systems

In the previous Chapter, we still kept open the question for the excitation location. As we can see in Figure 4-1, there are still two possibilities r_1 and r_2 for excitation and in this Section we will derive based on the related sensitivity functions which input location r_1 or r_2 is better.

We will first start by deriving the transfer function from r_2 to s first, i.e. $T_{r_2->s}$, because this excitation location is more common in practice more common. Afterwards we will compare this to $T_{r_1->s}$ by doing the same derivation. Let us now start by writing down the relationship between the signals u_{cmd} and s, applying the assumptions mentioned in the previous Section, we obtain:

$$s = G_{WFS}w_{atm} + G_{WFS}G_{DM}u \tag{5-1}$$

Since we are only looking into the relationship between r_2 and s, we will assume $w_{atm} = 0$. Substituting for u with $u = Cs + r_2$ gives us:

$$s = G_{WFS}G_{DM}(Cs + r_2) \tag{5-2}$$

$$s = G_{WFS}G_{DM}Cs + G_{WFS}G_{DM}r_2 \tag{5-3}$$

Substituting $G_{IM} = G_{WFS}G_{DM}$ and rewriting results in:

$$(1 - G_{IM}C)s = G_{IM}r_2 \tag{5-4}$$

$$s = \frac{G_{IM}}{1 - G_{IM}C}r_2 \tag{5-5}$$

Now, we shall do the same derivation for $T_{r_1->s}$ as well and finally compare both transfer functions to see which excitation location is a more rational and logic choice. Again we start off by writing down the relationship between u_{cmd} and s under the same assumptions:

$$s = G_{WFS}G_{DM}u \tag{5-6}$$

Substituting for u with $u = Cs + Cr_1$ gives us:

$$s = G_{WFS}G_{DM}(Cs + Cr_1) \tag{5-7}$$

$$s = G_{WFS}G_{DM}Cs + G_{WFS}G_{DM}Cr_1 \tag{5-8}$$

Substituting $G_{IM} = G_{WFS}G_{DM}$ and rewriting results in:

$$(1 - G_{IM}C)s = G_{IM}Cr_1 \tag{5-9}$$

$$s = \frac{G_{IM}C}{1 - G_{IM}C}r_1 \tag{5-10}$$

So when we write down the two transfer functions $T_{r_1->s}$ $T_{r_2->s}$ next to each other, we can clearly notice that $T_{r_1->s}$ is nothing more than a low-pass filtered version of $T_{r_2->s}$. This is due to therm C which represents an integrator:

$$T_{r_1->s} = \frac{G_{IM}C}{1 - G_{IM}C} \qquad T_{r_2->s} = \frac{G_{IM}}{1 - G_{IM}C} \tag{5-11}$$

This will have its effect on both the input and the output as well, because especially at higher frequencies we would have to use higher excitation to reach the same level of excitation at the output. Therefore, it is a clear choice to pick r_2 as our standard excitation location from now on. This is depicted in Figure 5-1 where also the assumptions as mentioned in the previous Section have been taken into account.

5-3 Finite dimensional parametrization of the input power spectrum Φ_r

An important part of our research is to determine a good parametrization for the infinite dimensional input power spectrum Φ_r, which is basically the decision variable of our optimization problem as described in Equation 4-6. In order to be able to solve this optimization

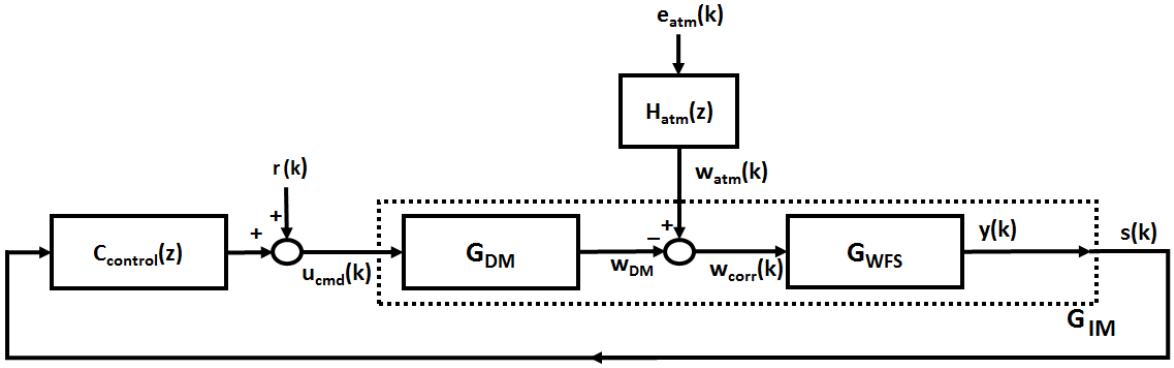

Figure 5-1: Final closed-loop identification setup for the telescope after assumptions and decision excitation location

problem using LMI optimization [44], we need to adapt a finite dimensional linear parametrization for our decision variable Φ_r.

In the papers published by Bombois and Gevers an FIR parametrization has been chosen [38] [43] [45]. We will show that for our application purposes this is not the best option. Therefore, we will explain why we specifically prefer a sinusoidal parametrization over an FIR parametrization.

In the following Subsections, we will explain both methods and sum the pros and cons. Subsequently, we will draw the final conclusion for our research purposes.

5-3-1 FIR parametrization

An FIR parametrization is represented by the following equation:

$$\Phi_r(\omega) = \sum_{k=-m}^{+m} R_k e^{j\omega k} = R_0 + 2\sum_{k=1}^{m} R_k cos(k\omega) \succeq 0 \quad \forall\omega, \tag{5-12}$$

where $R_{-k} = R_k$ are the decision variables and these variables can be interpreted as the autocorrelation coefficients of an FIR filtered Gaussian white noise signal. The scalar m is a user defined choice. Naturally, if we choose m large enough, the spectrum will have more freedom and flexibility to attain different excitation spectra. Also note that for the choice $m = 0$, we are simply defining a Gaussian white noise spectrum.

To guarantee the positivity of the spectrum we need to restrict the possible choices for the decision variables R_k by adding another LMI constraint [37]. For this purpose, the positive real lemma is applied. The existence of a symmetric Q satisfying the following constraints ensures that the spectrum Φ_r is indeed positive definite:

$$\begin{bmatrix} Q - A^T Q A & C^T - A^T Q B \\ C - B^T Q A & D + D^T - B^T Q B \end{bmatrix} \succeq 0, \tag{5-13}$$

where the matrices A, B, C and D are given as:

$$A = \begin{bmatrix} O_{1\times(m-1)} & 0 \\ I_{m-1} & O_{(m-1)\times 1} \end{bmatrix}, \quad B = \begin{bmatrix} 1 & 0 & ... & 0 \end{bmatrix}^T \tag{5-14}$$

$$C = \begin{bmatrix} R_1 & R_2 & ... & R_m \end{bmatrix}, \quad D = R_0/2 \tag{5-15}$$

An important advantage of this parametrization is the high numerical stability. However, this is at the cost of a very high computational load. This is because there is an additional LMI that needs to be solved. Especially for higher scales it becomes undesirable. Furthermore, since we are dealing with a sum of exponentials, this parametrization will not allow us to pinpoint the optimal frequency, which is basically one of the most important aspects of our research. This difference in pinpointing the optimal frequency between the two different parametrization methods has been depicted in Figure 5-2.

The smoothing nature of this method is an important drawback for our purpose of research in that it becomes more difficult to pinpoint the optimal frequency. It is possible to increase the value chosen for m, but combined with the high computational, it is not an option to increase the value of m too much. This causes not only difficulties with pinpointing the optimal frequency, but this also leads to less optimal solution. To understand this, one can simply try to look at the extreme case of $m = 0$, which equals Gaussian white noise. For this case, it can be easily understood that a big part of the excitation spectrum is unnecessary additional cost.

5-3-2 Multisine parametrization

A multisine parametrization is represented by the following equation:

$$\Phi_r(\omega) = \sum_{k=1}^{m} R_k \left(\delta(\omega - \omega_k) + \delta(\omega + \omega_k)\right) \succeq 0 \quad \forall\omega, \tag{5-16}$$

For the computational load criterion, clearly, the multisine method is much faster than the FIR method. This is simply because for the FIR method another extra LMI problem has to be solved in order to guarantee positive definiteness of the spectrum, while in the case of the multisine, it is simply a matter of constraining all amplitudes of the sinusoidals to be positive.

As for numeric stability, it appears that the multisine parametrization becomes less stable for higher sampling rates. This is because the solvers cannot distinguish the difference between two very close sinusoidals in terms of the information matrix. Therefore, in case of finer sampling, the difference is numerically too small to be taken into consideration by the solvers, which means that the problem has basically turned into a non-convex problem and, logically, this causes all the difficulties with the LMI solvers. For this reason, the FIR parametrization performs slightly better in terms of stability. However, since the multisine parametrization still performs perfectly fine for sample rates that are more than needed for our purpose, it is not necessary to rule out this method based on its numeric stability properties.

An important extra advantage of this method is that it is strong in pinpointing the optimal frequency as opposed to the FIR parametrization which is basically nothing more than a smoothed spectrum, especially for low m.

5-3-3 Final parametrization choice for our purpose

In this section we will summarize the advantages and disadvantages of both parametrization methods and make a final choice while keeping in mind the needs for our research purpose. Therefore, we will have to carefully select the criteria to choose the best method for our purposes.

In any case, it is important to have numerical stability and an FIR parametrization is better in terms of numerical stability than a multisine method. However, this problem only appears for extreme fine sampling and, thus, a multisine parametrization is still applicable to our problem as long as the sampling is not taken much higher than necessary.

Another important criterion to asses our parametrization method is the computational load. It is undesirable to have high computational load for our purpose. This is first of all because different scenarios will be investigated and, thus, calculation time to obtain results is important. There is also the aspect of available computational power at ESO. For the method to be applicable for ESO, it must not have high computational load, due to the limited resources.

The ability to pinpoint the optimal frequency is for our purpose also an option that we cannot miss out on. It is clear that the FIR method leads to smoothed spectra while the multisine method picks out a single frequency or a set of single frequencies. This also leads us to our last criterion which is the cost itself. A smoothed spectrum, as is the case for the FIR method, leads naturally to higher cost.

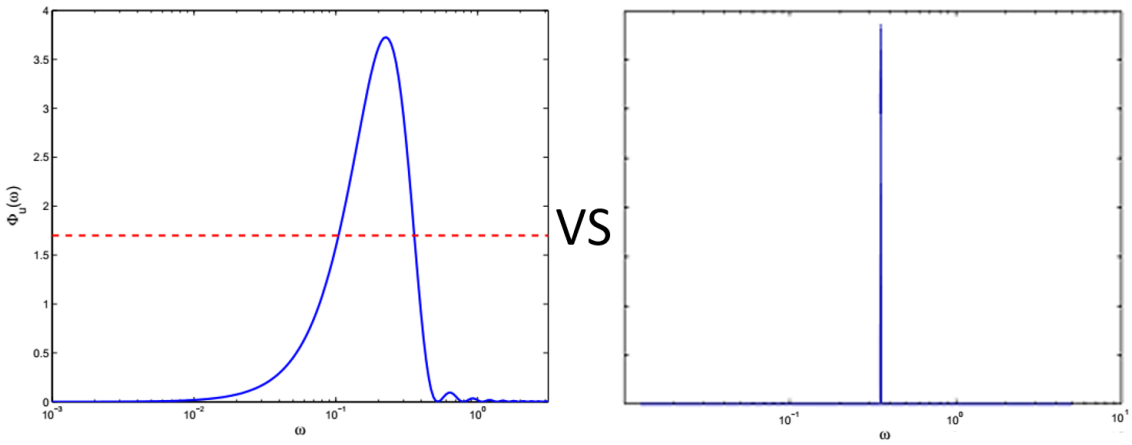

Figure 5-2: The differene in pinpointing the optimal frequency between an FIR parametrization and a multisine parametrization

Table 5-1: Summary and comparison of the advantages and disadvantages of both FIR and multisine parametrization methods

	FIR low m	**FIR high m**	**multisine**
numerical stability	++	++	+-,+
low computational load	-	- -	++
pinpointing strength	- -	-	++

5-4 Convex formulation of the accuracy constraint

In the previous Section, we have taken a first step to apply least cost optimization in practice. There are, however, still some other important issues if we look back at the constraints as formulated in the optimization problem in Equation 4-6. We can see that the accuracy constraint $\alpha\sqrt{\lambda_1(T(e^{j\omega},\theta)P_\theta T(e^{j\omega},\theta)^T)} < r_{adm}$ is first of all not a function of the decision variable $\Phi_r(\omega)$. Another essential requirement that has to be met is that the accuracy constraint becomes an affine function of the decision variable $\Phi_r(\omega)$. Furthermore, we can also still see that there are an infinite number of constraints.

In the following subsections, we shall first discuss how we can turn the current accuracy constraint into an affine function of the decision variable using the expression for the information matrix [34] [35] and the Schur complements [44]. After this, we will formulate our final convex optimization problem, which will be followed by a discussion on how to solve the issue of still having an infinite number of constraints.

5-4-1 Reformulating accuracy constraint as an affine function in Φ_r

A function in terms of the decision variable can be obtained by substituting the following expression for the information matrix, the inverse of P_θ [35]:

$$\begin{aligned} P_\theta^{-1} = &\frac{N}{\sigma_e^2}\frac{1}{2\pi}\int_{-\pi}^{+\pi} F_r(e^{j\omega},\theta_0)F_r^*(e^{j\omega},\theta_0)\Phi_r(\omega)d\omega \\ &+ \frac{N}{\sigma_e^2}\frac{1}{2\pi}\int_{-\pi}^{+\pi} F_n(e^{j\omega},\theta_0)F_n^*(e^{j\omega},\theta_0)\sigma_e^2 d\omega, \end{aligned} \tag{5-17}$$

where $F_r(z,\theta_0) = \frac{\nabla_G(z,\theta_0)}{(1+CG_0)H_0}$ and $F_n(z,\theta_0) = -\frac{C}{(1+CG_0)}\nabla_G(z,\theta_0)$. Of course, in open-loop, due to the absence of feedback, i.e. $C = 0$, these expressions simplify into $F_r(z,\theta_0) = \frac{\nabla_G(z,\theta_0)}{H_0}$ and $F_n(z,\theta_0) = 0$.

In the expression for the information matrix above, for our research purposes, without loss of generality, information on possible parameters of $H(\theta)$ have been discarded and, thus, we solely considered the part of the information matrix related to the plant parameters.

Now remains the rewriting of the accuracy constraint $\alpha\sqrt{\lambda_1(T(e^{j\omega},\theta)P_\theta T(e^{j\omega},\theta)^T)} < r_{adm}$ into an affine function of Φ_r, which can be done using the Schur complements [44] [43]:

$$\begin{aligned} P_\theta^{-1} &\succeq R_{adm}(\omega) \\ &\succeq \frac{\alpha^2}{r_{adm}^2}T(e^{j\omega},\theta)^T T(e^{j\omega},\theta) > 0 \quad \forall\omega \end{aligned} \tag{5-18}$$

Therefore, the final formulation of the convex least cost optimization problem becomes:

$$\min_{\Phi_r} \frac{1}{2\pi}\int_{-\pi}^{+\pi}\Phi_r(\omega)d\omega \quad s.t. \quad \Phi_r \succeq 0 \quad and \quad s.t. \quad P_\theta^{-1} \succeq R_{adm}(\omega) \quad \forall\omega, \tag{5-19}$$

where P_θ^{-1} and R_{adm} are given in Equation 5-17 and 5-18 respectively.

If we define the cost to be the deterioration of the normal closed-loop operation, the cost part of the final formulation becomes different:

$$\min_{\Phi_r} \frac{1}{2\pi} \int_{-\pi}^{+\pi} \frac{|G|^2}{|1+GC|^2} \Phi_r(\omega) d\omega \quad s.t. \quad \Phi_r \succeq 0 \quad and \quad s.t. \quad P_\theta^{-1} \succeq R_{adm}(\omega) \quad \forall \omega, \quad (5\text{-}20)$$

5-4-2 infinite number of constraints

The optimization problem as formulated in Equations 5-19 5-20 is still not numerically solvable, because there are an infinite number of constraints. This for the reason that the accuracy constraint must hold for all possible ω. The simplest solution to overcome this problem is simply by sampling the frequency ω [43].

This approach does require, however, among other things, numerical integration of the information matrix, which brings along numerical problems of its own. These issues will be discussed and solved for in Section 5-6-1.

5-5 Costless closed-loop identification in depth

In this Section, we will have an in depth study of costless identification. We will start off with deriving necessary and sufficient conditions for costless identification to be possible for our AO system in question, which we have modeled using a Box-Jenkins model structure. After that, we will derive the accuracy capabilities of costless identification based on the information matrix as defined earlier in Equation 5-17. Finally, we will analyze whether more disturbance has a positive or negative effect on the accuracy of the experiment.

5-5-1 Conditions for costless identification for AO systems specifically

Earlier in Section 3-4-2, we have explained in which cases costless identification is possible for the Box-Jenkins model structure. It was explained that if and only if either $n_x + n_k > n_d + n_f$ or $n_y > n_b + n_d$ the information matrix is positive definite.

This means that in our case, since AO systems usually use a simple integrator as controller and since AO systems are usually modeled as a simple gain, costless identification is applicable to the system as long as we try to identify a scalar Interaction Matrix, which represents the dc gain of our plant.

5-5-2 Information content and accuracy capabilities of costless closed-loop identification

In the previous subsection, we looked into the necessary and sufficient conditions for costless identification to be possible. Now we will look into the amount of information that costless identification can provide us. To do this, we will look again into the expression for the information matrix in Equation 5-17. Since there is no explicit external excitation, i.e. $\Phi_r(\omega) = 0$, the expression for the information matrix simplifies to:

$$P_\theta^{-1} = \frac{N}{\sigma_e^2}\frac{1}{2\pi}\int_{-\pi}^{+\pi} F_n(e^{j\omega},\theta_0)F_n(e^{j\omega},\theta_0)^*\sigma_e^2 d\omega \tag{5-21}$$

Since we have already established the requirements for costless identification we know that the matrix resulting from the integral $\int_{-\pi}^{+\pi} F_n(e^{j\omega},\theta_0)F_n(e^{j\omega},\theta_0)^* d\omega$ will be positive definite. The duration of the experiment can be scaled up unlimitedly, this means that, theoretically, costless identification is able to provide unlimited accuracy, because it should be clear that as $N \to \infty$ also $P_\theta^{-1} \to \infty$. Thus, if more accuracy is needed, we can simply scale up the experiment duration N, which represents the number of samples.

So we have established that costless identification can provide unlimited accuracy. However, what is needed to extract this information? This can be understood by looking back at Equation 3-21:

$$\epsilon(k,\theta) = y(k) - \hat{y}(k|k-1,\theta) = H^{-1}(q^{-1},\theta)[y(k) - G(q^{-1},\theta)u(k)] \tag{5-22}$$

In the very definition of the prediction error, accurate information regarding the disturbance H is needed. As explained in Section 3-2-3, consistency problems occur as soon $H \notin \mathcal{H}$. Thus, although costless identification can provide us with sufficient information, whether we are able to extract this information depends on how good we are able to capture the dynamics of atmospheric turbulence in an accurate model. Further analysis on this topic will be in Section 7-3.

5-5-3 Does more disturbance power lead to more or less information content?

There is an interesting and peculiar paradox with costless identification, which is the role of the disturbance or the noise. In regular open-loop identification, less disturbance or noise is always better, because this aids the accuracy of the experiment. However, with costless identification the disturbance does not solely play a "bad" role, because at the same time it is our single source of excitation, and thus also our single source of information.

Naturally this leads to the following interesting question. Does more power in the spectrum of the disturbance lead to better or worse accuracy in costless identification experiments? Or what happens when we the disturbance has a different spectrum.

First of all, more disturbance seems to be a "bad" thing. No one desires disturbance or noise to corrupt their experiment. However, at the same time, this leads to more information, which is "good". The same line of reasoning can be followed for less disturbance. The true answer on this question is: ***It does not matter!***.

To understand how this works exactly, we will look back to the information matrix as defined for costless identification experiments in Equation 5-21 and work out the expression:

$$\begin{aligned} P_\theta^{-1} &= \frac{N}{\sigma_e^2}\frac{1}{2\pi}\int_{-\pi}^{+\pi} F_n(e^{j\omega},\theta_0)F_n(e^{j\omega},\theta_0)^*\sigma_e^2 d\omega \\ &= N\frac{1}{2\pi}\int_{-\pi}^{+\pi} F_n(e^{j\omega},\theta_0)F_n(e^{j\omega},\theta_0)^* d\omega \\ &= N\frac{1}{2\pi}\int_{-\pi}^{+\pi} \left(\frac{C}{(1+CG_0)}\nabla_G(z,\theta_0)\right)\left(\frac{C}{(1+CG_0)}\nabla_G(z,\theta_0)\right)^* d\omega \\ &= N\frac{1}{2\pi}\int_{-\pi}^{+\pi} \left|\frac{C}{(1+CG_0)}\nabla_G(z,\theta_0)\right| d\omega \end{aligned} \tag{5-23}$$

From the second line, it already becomes clear that the disturbance itself plays no role whatsoever in the achievable accuracy. When working out this expression even further, we see that only the plant G and the controller C are decisive elements that influence the achievable accuracy.

5-6 Overcoming numerical issues

An important part of the research was invested into solving numerous numerical issues. In this Section, two important factors needed for the stability of LMI solvers such that convergence is possible. In the last Subsection, since different solvers have different performance, we will review three different LMI solvers which have been applied during our research namely SeDuMi, SDPT3 and MOSEK.

5-6-1 Numeric integration of the information matrix

To understand what kind of problems might occur when numeric integration is applied to obtain the information matrix, we need to look back at the definition of the information matrix in Equation 5-17. For simplicity's sake and without the loss of generality, we shall only look at an open-loop case, i.e. $F_r(z,\theta_0) = \frac{\nabla_G(z,\theta_0)}{H_0}$ and $F_n(z,\theta_0) = 0$:

$$P_\theta^{-1} = \frac{N}{\sigma_e^2}\frac{1}{2\pi}\int_{-\pi}^{+\pi} F_r(e^{j\omega},\theta_0)F_r(e^{j\omega},\theta_0)^*\Phi_r(\omega)d\omega \tag{5-24}$$

Now, let us zoom in more into the term $F_r(e^{j\omega},\theta_0)F_r(e^{j\omega},\theta_0)^*$, which we shall assume to be a 3×3 matrix, because for our research purposes we will eventually switch to a second order system with three free variables:

$$\begin{bmatrix} F_r(1)F_r(1)^* & F_r(1)F_r(2)^* & F_r(1)F_r(3)^* \\ F_r(2)F_r(1)^* & F_r(2)F_r(2)^* & F_r(2)F_r(3)^* \\ F_r(3)F_r(1)^* & F_r(3)F_r(2)^* & F_r(3)F_r(3)^* \end{bmatrix} \tag{5-25}$$

In the matrix above the blue diagonal entries are actual real entries, because we are multiplying a complex expression with its complex conjugate. However, if we start off in Matlab numerically from the very start, even these diagonal entries that should be real end up complex. This error continues of course in the integration and finally the LMI becomes unsolvable,

because we are trying to "compare" complex numbers with each other, which is clearly impossible.

One might be tricked into thinking that taking the real part or the absolute value of the final result will solve this problem. Unfortunately, the opposite is true. It appears that if we start off with unsimplified expressions in this matrix, we create an error that deteriorates the accuracy at each iteration, thereby making the error bigger with each step.

For this reason, it is essential to utilize the Matlab Symbolic Toolbox to arrive at real and maximally simplified expressions for the entries. It is important to explicitly enforce a real expression in the Toolbox and also give explicit commands about the type of expression we need to arrive at. For the diagonal entries for example, we had to explicitly specify the expression we need to arrive at as follows:

$$F_r(i)F_r(i)^* = Re(F_r(i))^2 + Im(F_r(i))^2, \tag{5-26}$$

which needed to be calculated in three separate steps, first by calculating the real part, then the imaginary part, then finally by summing the squares of these expressions.

An even more interesting issue is with the non-diagonal entries of the matrix above. These are complex expressions and this calls for problems with numeric integration. It can be proven, however, that the non-diagonal entries are real symmetric and complex anti-symmetric. Once knowing this fact, since the interval of the integral $[-\pi, +\pi]$ is also symmetric, we can already conclude that the complex part of the integral will disappear eventually anyway. Therefore, instead of taking $F_r(i)F_r(j)^*$, with $i \neq j$, we took the real part of this expression. This has been explicitly enforced in the Matlab Symbolic Toolbox as follows:

$$Re(F_r(i)F_r(j)^*) = Re(F_r(i))Re(F_r(j)) + Im(F_r(i))Im(F_r(j)) \tag{5-27}$$

5-6-2 Data scaling for the numeric stability of the solvers

For numeric stability purposes, data scaling is important. In the online Google Groups of Yalmip, Johan Löfberg, the creator of YALMIP, spent numerous topics on the importance of data scaling for stability.

To understand this, we will provide a simple example. Suppose we are dealing with the following simple optimization:

$$\min_x \quad x \quad s.t. \quad 10^9 x \geq 10^5 \tag{5-28}$$

By simple observation, we can already conclude that the solution is given by $x = 10^{-4}$. In practice, however, numerical problems are to be expected, because the order of x is too small in comparison with the other constraint values. This creates high numerical sensitivity, because small rounding errors can now have a magnified effect on the solution. Due to this reason, it is difficult, sometimes even impossible, for the solver to converge to a correct solution.

For this purpose, in our Matlab code, a scaling parameter is included in order to lessen the difference in order of magnitude.

5-6-3 Review LMI solvers

In our research, three different LMI solvers have been used: SeDuMi, SDPT3 and MOSEK. Our experience with the three packages has been quite different and, therefore, we want to include a small summary of what we have experienced in terms of speed, stability and accuracy, cost, and error feedback.

SeDuMi is in our opinion the best among the three packages. Due to its strict solver policy, it is the most stable solver. SeDuMi gives an error even if something might go wrong. SDPT3 is in some cases for example able to solve an LMI with unscaled data. In the same case, SeDuMi would directly throw an error. However, there are also cases in which SDPT3 tries to solve the problem and comes up with a completely wrong solution and even gives the message "successfully solved", while SeDuMi throws an error. Therefore, when SDPT3 is compared with SeDuMi in terms of stability and accuracy, we can clearly say that SeDuMI is the winner. In terms of speed both SDPT3 and SeDuMi are the big winners, although SDPT3 is slightly faster each time. Since both, SeDuMi and SDPT3 are free packages this is also good. Finally, there is the issue of error feedback. Although SeDuMi is the one throwing an error easily, in comparison with SDPT3 it does not give helpful feedback.

We have kept MOSEK for the last, because we want to be quite short about it. Although MOSEK is a commercial package, it looses on all fronts. In most cases, MOSEK either produces a result that is complete rubbish or throws an error with very vague error feedback while both the other solvers are able to successfully solve the problem.

Chapter 6

Results and interpretation least cost identification AO system

In this Chapter, we will present and explain the resulting least cost excitation spectra for different systems that represent our AO System. In all Sections, the resulting spectra have been normalized in order to fit into one plot together with the other responses.

First, in Section 6-1, we will derive representative plant and disturbance models to apply our method to. We will have a separate plant model for our AO system in question which is the VLT of ESO, which will be based on the measurements we received from ESO. However, since we want our results to be applicable for other AO systems as well, we will derive in total three systems that are representative for an AO system.

For each system in both open-loop and closed-loop, a separate Section will be devoted in which the resulting least cost excitation spectrum will be explained and linked to response(s) of the system. This can thus be linked to the response of the plant $G_{1,2,3}$, the disturbance H or in closed-loop to the closed-loop response of the system $G_{cl} = \frac{G}{1+CG}$.

Initially, in order to build intuition for the least cost identification method, we shall define the cost as the total energy of the excitation spectrum as defined in Equation 5-19, i.e. $\mathcal{J} = \frac{1}{2\pi}\int_{-\pi}^{+\pi} \Phi_r(\omega)d\omega$.

Although, this will provide us with important insights, it is still not our final goal. We are interested in the spectrum that deteriorates the closed-loop operation of the system as low as possible. In order to take this into consideration we have to change the cost into $\mathcal{J}_{cl} = \frac{1}{2\pi}\int_{-\pi}^{+\pi} \frac{|G|^2}{|1+GC|^2}\Phi_r(\omega)d\omega$, which represents the part of the of the output signal that is caused by the extra presence of the signal $r(k)$.

Therefore, in our final section 6-7, we shall look into the optimization problem as defined in Equation 5-20 for the underdamped second order resonance system $\mathcal{M}_2$ in closed loop, which is the most representative for AO systems.

In the same final Section 6-7, we will prove mathematically that the information-to-cost ratio solely depends on the disturbance $H(j\omega)$. Therefore, in our specific case, with a low frequency

disturbance coming from atmospheric turbulence, it is always best to excite the system at the highest possible frequency, which is in our case the Nyquist frequency.

6-1 Plant and disturbance modeling

In the following of this Chapter, we will need a model for the plant we want to research, but also a model for the temporal response of the disturbance.

The spectrum of the temporal response of atmospheric turbulence is given as follows in [46]:

$$W_\phi(f) = 0.033 C_n^2 \bar{k}^2 L v^{5/3} \left(f^2 + \frac{k_0^2 v^2}{4\pi^2} \right)^{-4/3} \tag{6-1}$$

This means that the spectrum has the following form:

$$|H(j\omega)|^2 = \frac{a^2}{(-(\frac{j\omega}{2\pi})^2 + b^2)^{4/3}} \tag{6-2}$$

The exponent 4/3 can be approximated by 1:

$$|H(j\omega)|^2 \approx \frac{a^2}{(-(\frac{j\omega}{2\pi})^2 + b^2)} \tag{6-3}$$

and since $|H(j\omega)|^2 = H(j\omega)H(-j\omega)$ this gives:

$$H(j\omega) = \frac{a}{\frac{j\omega}{2\pi} + b} \tag{6-4}$$

Therefore, $H(s) = \frac{\gamma s_0}{s+s_0}$. The measurements from the data coming from ESO show that $s_0 \approx 2\pi$ and $\gamma \approx 0.01$. For computational load purposes s_0 has been downscaled to 0.2π in our derivations.

As for the plant itself, we will consider three different systems. In Figure 2-7, we can clearly see that up to 180 Hz the gain of the plant is mainly straight. Therefore, the first approximation we will make is a simple unit delay gain system:

$$\mathcal{M}_1 = G_1(z,\theta) = gz^{-1} \qquad H(z) = \frac{\gamma s_0}{s+s_0}|_{s=\frac{z-1}{Tsz}} \qquad \theta = g \tag{6-5}$$

This representation is together with the representation below in Equation 6-6 the most common, because the interaction matrix of the DM is assumed to be static and thus contains no dynamics. These representation are also used by ESO for the controller of the VLT and also very commonly used by the AO community [11] [12] [13].

For frequencies above 180 Hz, we have no further measurement information, because our excitation signal was low-pass filtered. However, it is safe to assume that the DSM of the VLT is an underdamped second order resonance system just as other DMs, see for example

Figure 7 in [32]. Also from [47], we understand that the resonance frequency for the DSM of the VLT is above 500 Hz, which essentially approves the usage of both $\mathcal{M}_1$ and $\mathcal{M}_2$. The representation $\mathcal{M}_2$ is defined as below:

$$\mathcal{M}_2 = G_2(z,\theta) = g\frac{\omega_0^2}{s^2+2\zeta\omega_0 s+\omega_0^2}\Big|_{s=\frac{z-1}{Tsz}} \qquad H(z) = \frac{\gamma s_0}{s+s_0}\Big|_{s=\frac{z-1}{Tsz}} \qquad \theta = g, \tag{6-6}$$

Finally, since we want an even more general representation we will also consider the following in which not only the gain of the system is considered but other dynamics as well:

$$\mathcal{M}_3 = G_3(z,\theta) = g\frac{\omega_0^2}{s^2+2\zeta\omega_0 s+\omega_0^2}\Big|_{s=\frac{z-1}{Tsz}} \qquad H(z) = \frac{\gamma s_0}{s+s_0}\Big|_{s=\frac{z-1}{Tsz}} \qquad \theta = \begin{bmatrix} g & \zeta & \omega_0 \end{bmatrix}^T, \tag{6-7}$$

where $0.1 < \zeta < 1$ and to prevent numerical issues and high computational load ω_0 is chosen $1 < \omega_0 < 5$. The choice for ω_0 to be low ensures that there are not too many samples. Therefore, without loss of generality we have down-scaled our problem.

The controller in closed-loop experiments $C(z)$ is a pure integrator:

$$C(z) = \frac{\kappa}{1-z^{-1}}, \tag{6-8}$$

where κ is the gain of the controller.

6-2 Open-loop unit delay AO system

In Figure 6-1, the least cost excitation spectrum for the unit-delay plant G_1 in open-loop is presented.

We can notice that the optimal frequency ω_{opt} is at the Nyquist frequency. The reason for this should be quite clear, because the amount of information that the plant provides at each frequency is the same, but the disturbance is the lowest at the Nyquist frequency. Thus, it has clearly chosen for the location of the best SNR.

It should also not be a surprise that a single frequency is used because there is only 1 variable that needs to be identified. Each sinusoidal input provides information about the phase delay and amplitude gain at that specific frequency, which means that it gives 2 equations.

6-3 Open-loop second order AO system dc gain

In Figure 6-2, the least cost excitation spectrum for the underdamped second order resonance system G_2 in open-loop is presented.

We can observe that the optimal spectrum concentrates its power at the peak response of the plant G_2, which makes sense, because this is the location of the best SNR. The disturbance

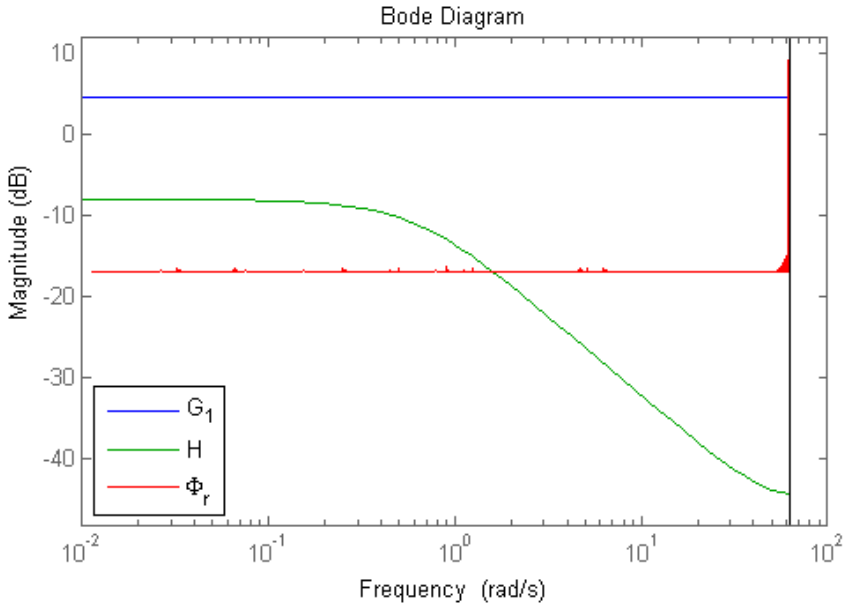

Figure 6-1: Least cost spectrum for G_1 in open-loop

H rolls off with a slope of -1 while the plant rolls off with a slope of -2. It was the other way around, the optimal frequency would still have been at the Nyquist frequency.

Furthermore, we can also notice that there is still one peak, which also still makes sense, because we are still trying to identify one variable.

6-4 Closed-loop second order AO system dc gain

In Figure 6-3, the least cost excitation spectrum for the underdamped second order resonance system G_2 in closed-loop is presented.

We can observe that the optimal spectrum now moves along with the magnitude peak of the closed-loop response G_{cl}. When the controller gain is zero, the response is and should be equal to the open-loop case. As we increase the gain, we notice the closed-loop response changing and the peak of the optimal excitation spectrum moves along with the peak magnitude of the closed-loop response. Again, it is clear that the optimal SNR is chosen for excitation. Furthermore, can still see one peak. It makes sense that the closed-loop structure does not change the number of peaks.

6-5 Open-loop full second order AO system

In Figure 6-4, the least cost excitation spectrum for the underdamped second order resonance system G_3 in open-loop is presented.

We can notice that there are now 2 peaks instead of one. This is because a single sinusoidal would provide 2 equations and thus we are only able to solve for 2 variables at most. Since we have three free variables in this case, we do need to have at least two peaks.

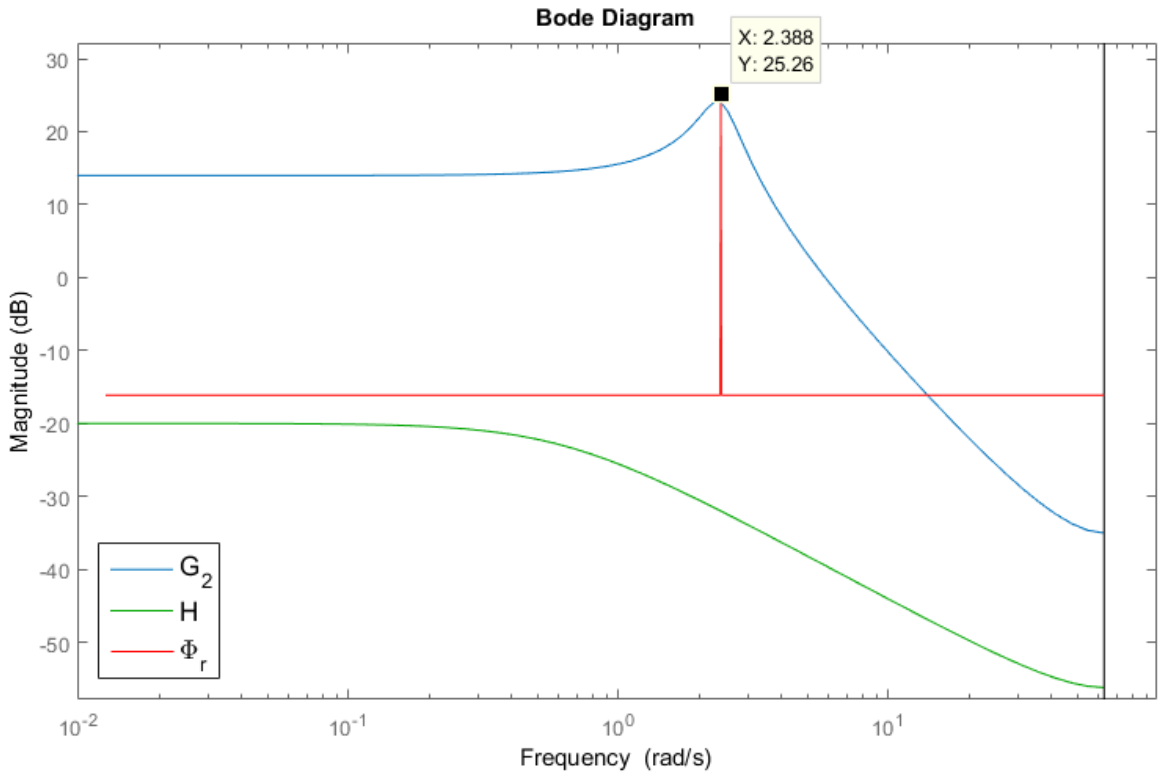

Figure 6-2: Least cost spectrum for G_2 in open-loop, $\zeta = 0.1$, $\omega_0 = 2.4\ rad/s$

The location of the sinusoidals is also an interesting point of discussion. They are placed at the locations where the second derivative the bode magnitude curve are zero. We would expect them to be as close as possible to the peak magnitude ω_0. However, on the other hand, the closer the sinusoidals will be to each other in terms of frequency, the more difficult it will be to distinguish them. Apparently, these two locations are the perfect balance of both.

It is important to note that the shape of the optimal excitation spectrum is independent of N.

In Figure 6-5, the least cost excitation spectrum for a critically damped second order resonance system G_3 in open-loop is presented. We can again notice two peaks, but the locations are now further apart. Apparently, when there is no obvious peak, it makes sense for the frequencies of the sinusoidals to be further apart. From this, we can conclude that the damping coeffecient ζ determines the distance between the sinusoidals mainly.

6-6 Closed-loop full second order AO system

In Figure 6-6, the least cost excitation spectrum for the underdamped second order resonance system G_3 in closed-loop is presented.

We can again notice that there are 2 peaks. This is to be expected, because closing the loop should not effect the minimum necessary sinusoidals to solve this problem. We can see that

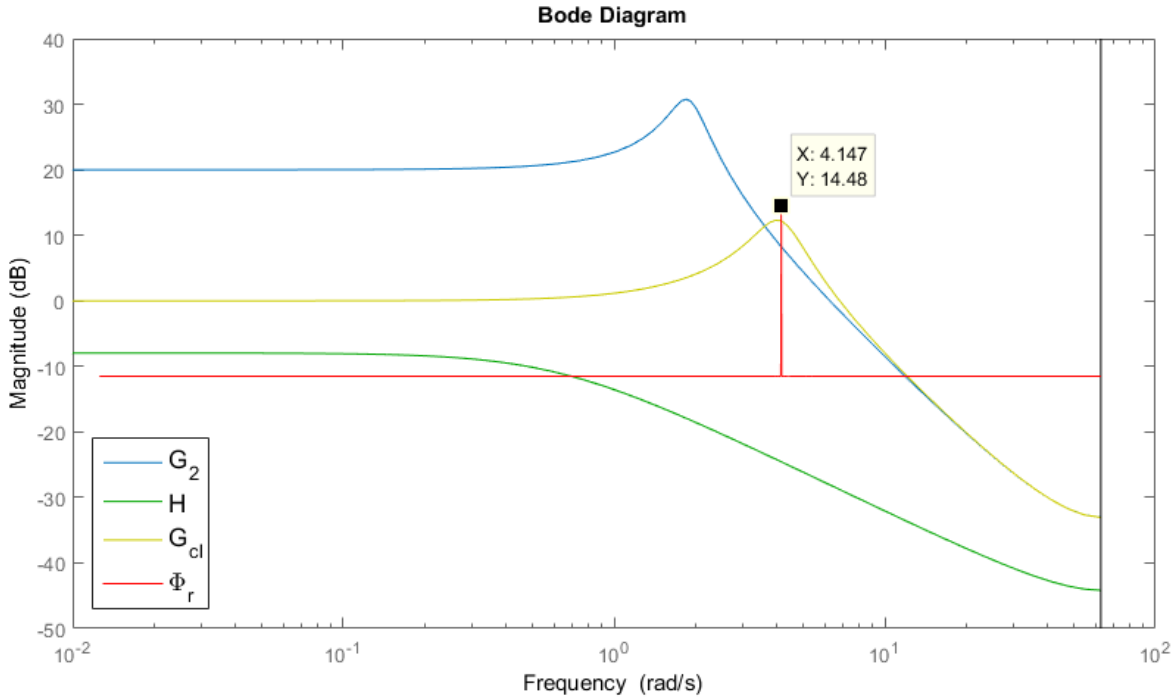

Figure 6-3: Least cost spectrum for G_2 in closed-loop, $\zeta = 0.1$, $\omega_0 = 1.9\ rad/s$, $\kappa = 0.09$

for closed-loop, the peak response of the open-loop and the peak response of the closed-loop are chosen as optimal locations.

6-7 Deterioration cost closed-loop second order AO system dc gain

In this Section, we will consider the deterioration of the normal closed-loop operation. The final and total convex optimization problem was given in Equation 5-20 and is given again below

$$\min_{\Phi_r} \frac{1}{2\pi} \int_{-\pi}^{+\pi} \frac{|G|^2}{|1+GC|^2} \Phi_r(\omega) d\omega \quad s.t. \quad \Phi_r \succeq 0 \quad and \quad s.t. \quad P_\theta^{-1} \succeq R_{adm}(\omega) \quad \forall \omega, \tag{6-9}$$

The resulting excitation spectrum for the closed-loop system G_2 is given in Figure 6-7. It is clear that the Nyquist frequency is chosen as the optimal one.

This selection is actually not surprising. In the following we will derive the information-to-cost ratio and show that it depends on $H(j\omega)$ solely. For this, we have to start from the expression of the information matrix as given in Equation 5-17. In our derivation, for simplicity's sake and without the loss of generality, we shall consider the continuous version:

$$\begin{aligned} P_\theta^{-1} = &\frac{N}{\sigma_e^2} \frac{1}{2\pi} \int_{-\infty}^{+\infty} F_r(\omega, \theta_0) F_r^*(\omega, \theta_0) \Phi_r(\omega) d\omega \\ &+ \frac{N}{\sigma_e^2} \frac{1}{2\pi} \int_{-\infty}^{+\infty} F_n(\omega, \theta_0) F_n^*(j\omega, \theta_0) \sigma_e^2 d\omega, \end{aligned} \tag{6-10}$$

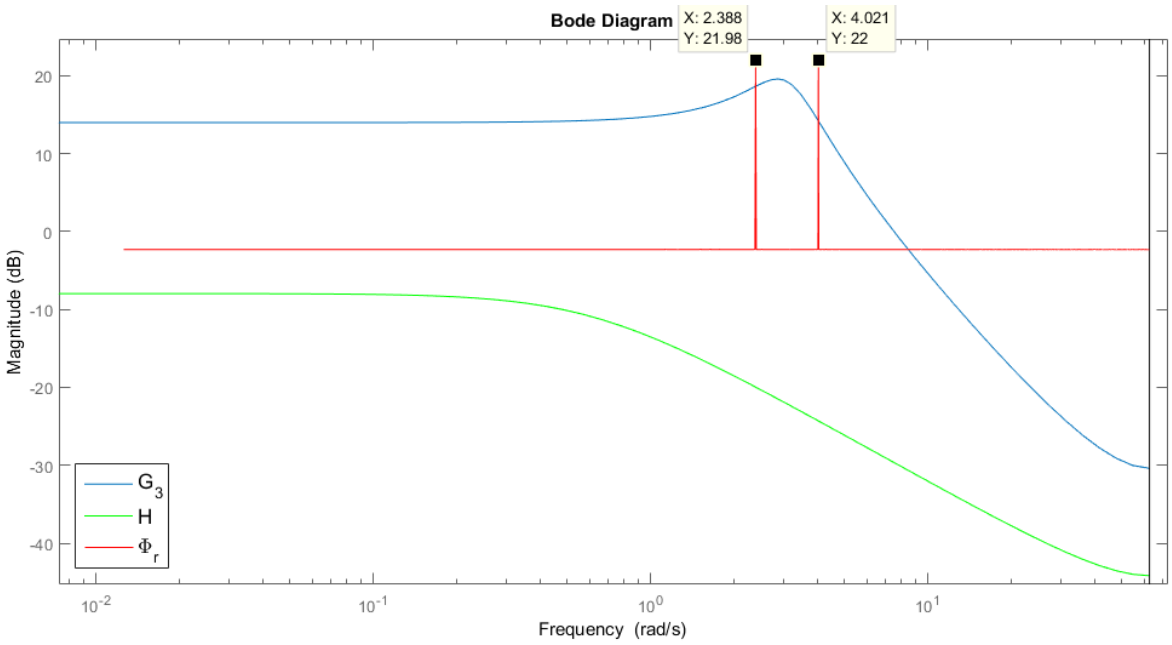

Figure 6-4: Least cost spectrum for underdamped second order system G_3 in open-loop, $\zeta = 0.2$, $\omega_0 = 3.1\ rad/s$

We know for a fact that in closed-loop identification of our AO when an external excitation signal is used and when short experiment durations are applied, the contribution coming from the disturbance is negligible. Therefore, the information matrix simplifies to the following expression:

$$P_\theta^{-1} \approx \frac{N}{\sigma_e^2}\frac{1}{2\pi}\int_{-\infty}^{+\infty} F_r(\omega,\theta_0)F_r^*(j\omega,\theta_0)\Phi_r(\omega)d\omega \tag{6-11}$$

The expression $F_r(\omega,\theta_0)$ for the system G_2 with the parameter vector $\theta = g$ becomes:

$$\begin{aligned} F_r(\omega) &= \frac{1}{(1+G_2C)H}\nabla_{G_2}(\omega) \\ &= \frac{1}{(1+G_2C)H}\frac{\delta G_2}{\delta g} \end{aligned} \tag{6-12}$$

and since $\frac{\delta G_2}{\delta g} = \frac{G_2}{g}$, this gives:

$$F_r(\omega) = \frac{1}{g}\frac{G_2}{(1+G_2C)H} \tag{6-13}$$

Thus the expression for $F_rF_r^*$ becomes:

$$F_rF_r^* = \frac{1}{g^2}\frac{1}{|H(\omega|^2}\frac{|G_2(\omega)|^2}{|1+G_2(\omega)C(\omega)|^2} \tag{6-14}$$

Substituting the expression for $F_rF_r^*$ in the information matrix gives:

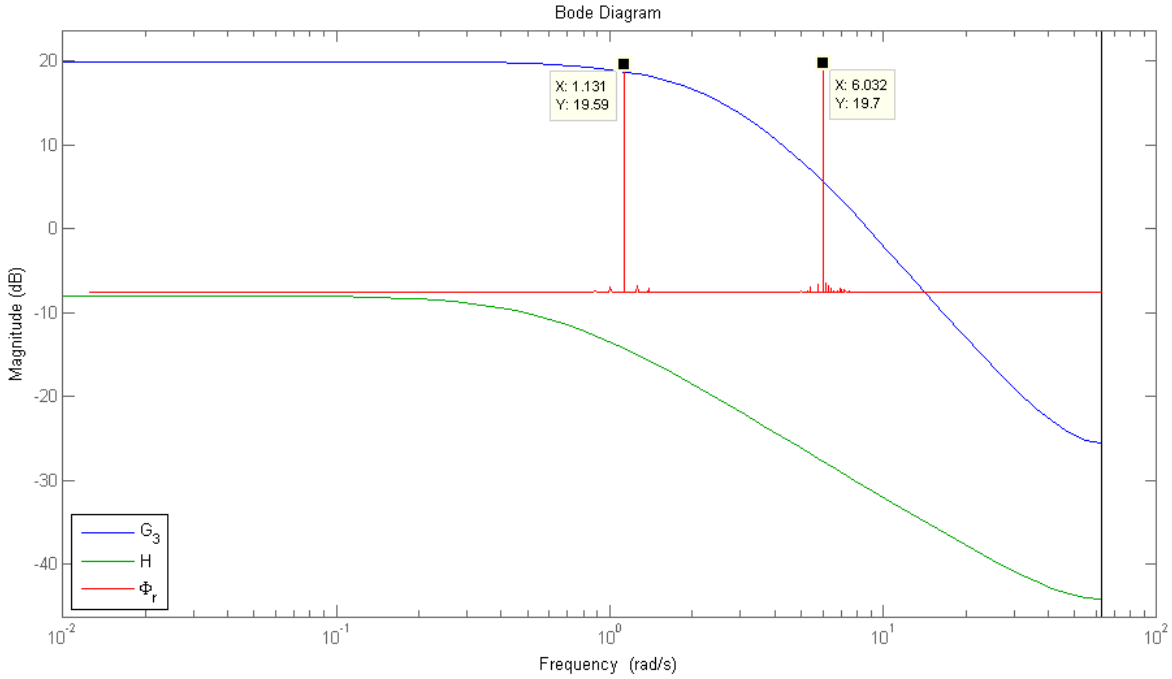

Figure 6-5: Least cost spectrum for critically damped second order system G_3 in open-loop, $\zeta = 1$, $\omega_0 = 3.1\ rad/s$

$$P_\theta^{-1} = \frac{1}{g^2}\frac{N}{\sigma_e^2}\frac{1}{2\pi}\int_{-\infty}^{+\infty}\frac{1}{|H(\omega)|^2}\frac{|G_2(\omega)|^2}{|1+G_2(\omega)C(\omega)|^2}\Phi_r(\omega)d\omega \tag{6-15}$$

Above we have the final expression for the information matrix, whereas the cost $\mathcal{J}_{cl}$ was defined as:

$$\mathcal{J}_{cl} = \frac{1}{2\pi}\int_{-\infty}^{+\infty}\frac{|G_2(\omega)|^2}{|1+G_2(\omega)C(\omega)|^2}\Phi_r(\omega)d\omega \tag{6-16}$$

From these expressions, we are able to derive the expressions for the information matrix and the cost in case of a single sinusoidal excitation signal at frequency ω_{sf}. These will be referred to as single frequency information matrix $P_{\theta,sf}^{-1}(\omega_{sf})$ and the single frequency cost $\mathcal{J}_{cl,sf}(\omega_{sf})$:

$$\begin{aligned} P_{\theta,sf}^{-1}(\omega_{sf}) &= \frac{1}{g^2}\frac{N}{\sigma_e^2}\frac{1}{|H(\omega_{sf})|^2}\quad \frac{1}{2\pi}\frac{|G_2(\omega_{sf})|^2}{|1+G_2(\omega_{sf})C(\omega_{sf})|^2}\Phi_{r,sf}(\omega_{sf}), \\ \mathcal{J}_{cl,sf}(\omega_{sf}) &= \qquad\qquad \frac{1}{2\pi}\frac{|G_2(\omega_{sf})|^2}{|1+G_2(\omega_{sf})C(\omega_{sf})|^2}\Phi_{r,sf}(\omega_{sf}), \end{aligned} \tag{6-17}$$

where $\Phi_{r,sf}(\omega_{sf})$ is the spectrum of a single sinusoidal signal at frequency ω_{sf}.

Now, we can derive the information-to-cost ratio (ICR) when a single sinusoidal excitation signal is applied to the system $G_2(\omega)$:

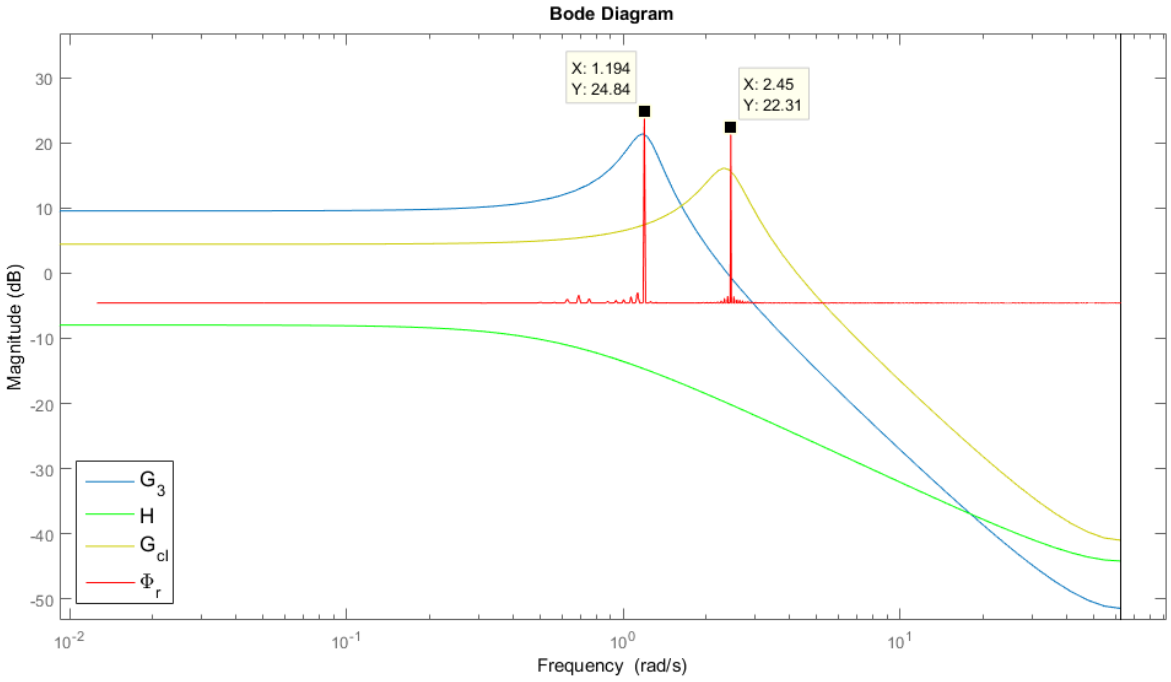

Figure 6-6: Least cost spectrum for underdamped second order system G_3 in closed-loop, $\zeta = 0.1$, $\omega_0 = 1.2$, $\kappa = 0.09$

$$\begin{aligned} ICR_{sf}(\omega) &= \frac{P_{\theta,sf}^{-1}}{\mathcal{J}_{cl,sf}} \\ &= \frac{1}{g^2}\frac{N}{\sigma_e^2}\frac{1}{|H(\omega)|^2} \end{aligned} \tag{6-18}$$

From the expression, we can observe that the single frequency information-to-cost ratio at a specific frequency is inversely proportional with the squared magnitude of the disturbance, i.e. proportional with $\frac{1}{|H(\omega)|^2}$. Furthermore, we can note that the expression for the information-to-cost ratio would be a scalar if $H(\omega)$ were to be a flat frequency independent transfer function.

For our specific case, in which we are dealing with low frequency disturbance coming from atmospheric turbulence, we are able to deduce that the Nyquist frequency is the optimal frequency for the single frequency information-to-cost ratio. This means that the result as shown in Figure 6-7 is a general result for second order systems with low frequency disturbance and, thus, for the new generation AO systems with a DSM such as the ELT and VLT of ESO, the best possible excitation frequency will always be the Nyquist frequency as long as they consider solely the deterioration of the output as the definition of their cost.

In practice it might be necessary to implement a simple additional constraint into the optimization problem due to saturation limits of the input, because it is possible that the magnitude of the system has become so small at the Nyquist frequency that the input reaches its saturation limit. The additional constraint will simply lower the excitation frequency up to a point where the magnitude of the system is large enough to prevent saturation of the input.

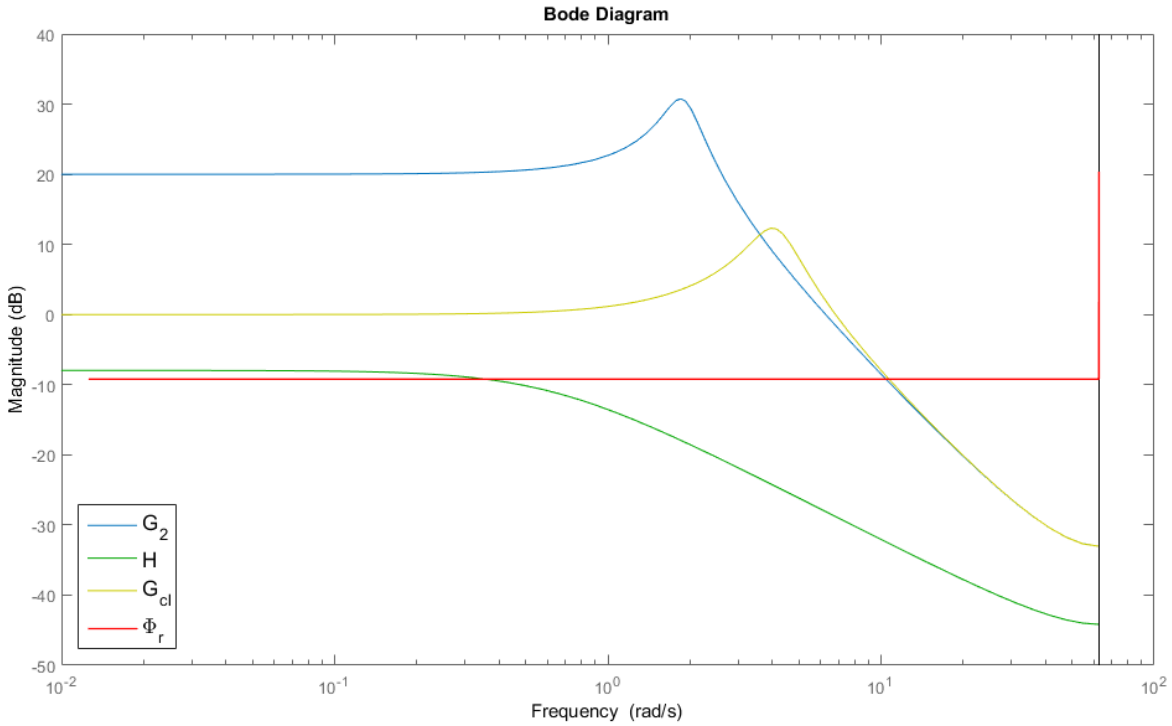

Figure 6-7: Least **deterioration** cost spectrum for G_2 in closed-loop, $\zeta = 0.1$, $\omega_0 = 1.9$, $\kappa = 0.09$

6-8 Final conclusion

For the identification of the static gain of closed-loop second order resonance systems in general, we have proven that the per frequency information-to-cost ratio is inversely proportional with the squared magnitude of the disturbance $H(\omega)$, i.e. proportional with $1/|H(\omega)|^2$.

In our specific case, in which are trying to calibrate the IM of an AO system and in which we are dealing with atmospheric turbulence, that has a low pass filtered character, the Nyquist frequency is the optimal frequency for excitation in terms of least disturbing the closed-loop operation.

Chapter 7

Discussion and evaluation

Up to now, we have presented and interpreted the meaning of the results in the light of our current research. However, scientifically it is important to present a critical attitude even towards your own results. In this Chapter, we will highlight our method from different perspectives, which were not highlighted before or were not considered because of the utilized assumptions. This will also lead to a number of suggestions and recommendations for future research, which will be explained in the related Sections.

As such, we shall first start off our discussion with robustness issues. Up to now, we have assumed "perfect" knowledge of our plant, and we have designed our excitation spectra accordingly. However, in practice it is never possible to perfectly know the system. Therefore, in the following Section, we shall discuss different methods on how to robustify the least cost experiment design method.

After this, we will continue our discussion by reconsidering our choice for the parametrization method, this time in view of a MIMO identification.

7-1 How to robustify the optimal experiment design procedure?

There is an important bottleneck inherent to all experiment design methods used in system identification, which is that the optimal experiment is naturally based on knowledge of the true system [35]. Since this is not available yet, designing the true optimal experiment is impossible. Therefore, as described in the previous Chapter initial estimates are taken to serve as a basis for the experiment design. When doing this, one should take care of doing this in the robust sense, because the initial estimate also has an uncertainty which affects, of course, the experiment design. The more information we have about the true plant, the closer we can get to the true optimal experiment. As long as perfect knowledge is not present, we have to ensure our experiment deals with the worst-case scenario by taking this into account.

There are currently two different methods available in literature to deal with robustness. First of all, there is so called adaptive design, which basically suggests taking the road of iterative

experiment design. As soon as new information about the system is available, this will be taken into account in the excitation signal, so that the spectrum of the excitation signal is basically optimized on-the-go [48] [49] [50].

Another method is a two-step procedure in which the uncertainty in the first step is taken into account 7-1 [51], [52], [53]. In this method, we adapt our already existing design procedure to encompass for the uncertainty of the initial parameter estimates, which are in actuality stochastic values. In the adapted design procedure, the stochastic nature of the parameter is taken into account by considering a domain of possible values instead of just one point. This has been shown in Figure 7-1 for a hypothetical two-dimensional estimate $\hat{\theta}_N$.

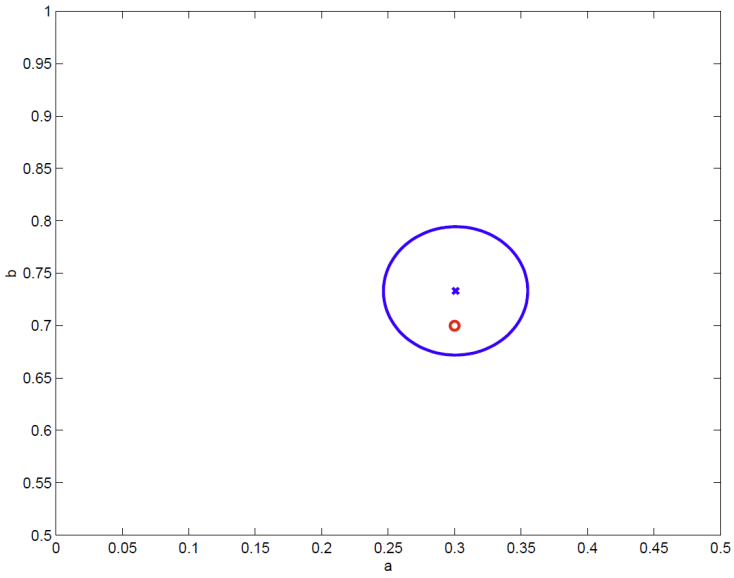

Figure 7-1: The estimate $\hat{\theta}_N$ (blue cross) along with its 95% uncertainty region, the ellipsoid U and true value (red circle) in the parameter space

The idea is that the initial estimate $\hat{\theta}_{init}$ is contained inside a set Θ, in practice this will be with a certain probability as shown with the 95% uncertainty region in Figure. Now, instead of designing the experiment solely based on the inaccurate $\hat{\theta}_{init}$, we choose to design the optimal experiment to account for the worst-case scenario inside the whole set Θ. So we choose a design criterion $f(P^{-1}(\theta), \theta)$ and optimize for the excitation spectrum such that it can account for all possible parameters within the set, thus $f(P^{-1}(\theta), \theta)$ over Θ.

After we adapt our original optimization problem with the method above, we will need to include the worst-case $\theta \in \Theta$ into our optimization. After this is included as well, the imposed optimization problem for the input $r(k)$ becomes:

$$\min_{\Phi_r} \max_{\theta \in \Theta} \frac{1}{2\pi} \int_{-\pi}^{+\pi} \Phi_r(\omega) d\omega \quad s.t. \quad \alpha \sqrt{\nabla_G(e^{j\omega}, \theta) P_\theta \nabla_G^T(e^{j\omega}, \theta)} < r_{adm} \tag{7-1}$$

7-2 MIMO considerations for the parametrization method

Up to now we have considered four different criteria which are computational load, numeric stability, pinpointing capability of the optimal frequency and, related to the pinpointing capability, the final cost. These were the most important criteria for our current research purposes. However, for further future research, it might also be interesting to consider the parametrization method in the light of MIMO systems, because there is an important difference compared with the SISO case, which is that it is not possible to excite interacting channels at the same instance with the exact same signal.

To understand this more properly, six different channels of a hypothetical AO system have been depicted in Figure 7-2. We can notice that, except for actuator 1 and actuator 6, all actuators influence each others channel. Therefore, identification is not possible when e.g. actuator 1 and actuator 2 are excited with the same signal at the same time, because it is impossible to differentiate the signals from each other.

This directly causes difficulties for the applicability of the current parametrization methods in MIMO closed-loop, because for the SISO case we are presented with a set of single optimal frequencies without any further phase information.

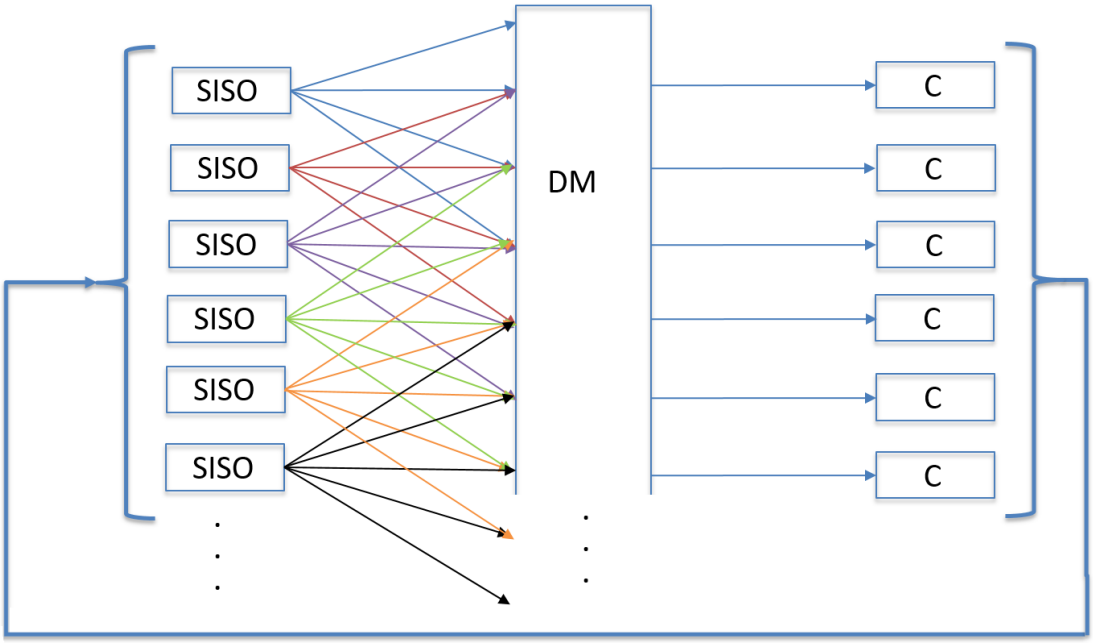

Figure 7-2: Effect of parallel excitation of interacting channels

For future work, it might be necessary to extend the basis with more information such as phase information for the multisine method. In that case, we can produce two sinusoidals at the same frequency with a phase shift of 90°, such that it becomes possible to excite neighbouring actuators without possible interference.

Also, it is interesting to notice that AO systems are locally coupled, but globally decoupled systems. This is depicted in Figure 7-3. This gives opportunities for sequential excitation of the actuators without any chance of interfering channels.

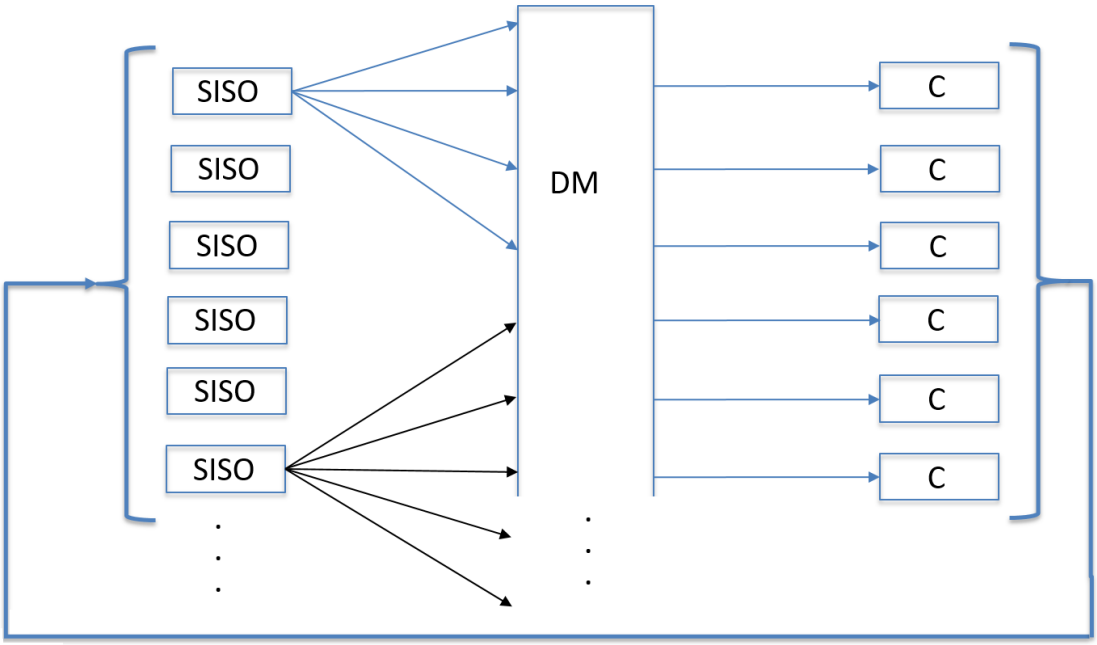

Figure 7-3: Sequential excitation of non-interacting channels

7-3 Modeling the disturbance characteristics

Theoretically, in closed-loop the disturbance can provide sufficient accuracy in case identifiability is given. However, although the information is present, in order to extract that information we do need accurate information on the disturbance characteristics. In our research, we did not investigate how accurately the applied model captures the true disturbance characteristics. Neither did we spent time on more accurate, i.e. higher order, modeling possibilities of the disturbance.

For future work, it is interesting to further research the potential use of costless identification. For this purpose, we would need to investigate how well we are able to capture the dynamics of atmospheric turbulence, and how well the available information allows itself to be extracted with this approximate model.

Is it possible to correct for certain mis-registration parameters by means of an approximate model? As explained earlier, in case of a too big modeling error consistency problems as described in Section 3-2-3, will arise. If it appears that, in any case, sufficiently accurate modeling is not possible due to the complex characteristics of atmospheric turbulence, it is advisory not to choose for costless identification. So unless sufficiently accurate information about the characteristics of the atmospheric turbulence at the specific location and time are present, it is not the road map to choose for, because without this information we are not able to extract the information that is present.

Chapter 8

Conclusion

This final Chapter will discuss the main conclusions that can be drawn from our study. For this purpose, we will of course keep in mind the boundaries of our research, which were highlighted in the previous Chapter, and make sure not to draw any expeditious conclusions.

The motivation for this research was the development of the new generation integrated AO systems with a Deformable Secondary Mirror (DSM) such as the VLT and the ELT. These new AO systems are much more sensitive to external factors and therefore need regular calibration as opposed to the older systems. Due to this, ESO wants to do the identification experiment necessary for the calibration in closed-loop and in a manner that minimally disturbs the observations coming from the telescope. In control-theoretical terms this means that the normal closed-loop operation of the telescope should be disturbed as low as possible for the identification experiment.

Up to now, only one serious proposal was made to solve for this problem by Béchet and Kolb. In our study, we have first of all proven that their approach is fundamentally wrong and that it will lead to the identification of the static gain of the inverse controller.

Furthermore, the research conducted at TNO for this thesis led to the proposal of a new calibration strategy. This strategy, which is a paradigm for parametric prediction error identification recently developed by the system identification community, designs the excitation signal in such a way that the corresponding experiment is the least cost, i.e. least intrusive, for the underlying system while guaranteeing a predefined level of accuracy. The cost can be defined in several ways depending on the application. In open-loop, a straightforward definition for the cost is the total energy of the input signal, which is a combination of the total power of the input and the experiment duration. For our purpose however, since we are not specifically interested in limiting the power of the input signal, this cost has been defined as the total power of the perturbations at the output of the system induced by the excitation signal. Minimizing this cost will ensure that the normal closed-loop operation, and thus the observations coming from the telescope, are minimally distorted.

For the identification of the static gain of closed-loop second order resonance systems in general, we have proven that the per frequency information-to-cost ratio is inversely proportional

with the squared magnitude of the disturbance $H(\omega)$, i.e. proportional with $1/|H(\omega)|^2$. In our specific case, in which are dealing with atmospheric turbulence, the disturbance has a low pass filtered character. This means for the new generation AO systems such as the VLT and ELT of ESO, that the Nyquist frequency is the optimal frequency for excitation in terms of least disturbing the closed-loop.

Finally, we have also shown that, in theory, if accurate information on the disturbance characteristics is available and if time allows, it is possible to achieve unlimited accuracy using the excitation originating from the disturbance signal if we want to identify the static gain of closed-loop second order resonance systems.

Appendix A

Modeling Atmospheric Turbulence for Simulation

There are multiple methods available in literature for modelling atmospheric turbulence in order to simulate an AO system. These can be roughly divided into two main methods. The first is based on using the spectral power spectrum of atmospheric turbulence, while the others are called covariance methods [54]. The spectral power spectrum based methods rely on the fact that the information from the frequency domain can be translated back into the spatial domain. The covariance methods are directly in the spatial domain. Here, the covariance matrix of atmospheric turbulence is used to generate realizations [55].

The method based on filtering white Gaussian noise in the spectral domain in order to obtain spatial information by means of Fourier transformation was first proposed by McGlamery [56] and improved on by several researchers. Although several other methods were created, by far this stayed the most popular method [57].

In [56], [57] and others, the Kolmogorov model for atmospheric turbulence is used which has a non-integrable pole at zero. Our method is based on their theory but improves the method by using the Von Karman model for atmospheric turbulence.

We start with the Von Karman spectrum for atmospheric turbulence:

$$\Phi(f,z) = 0.033 C_n^2(z)(f^2 + f_0^2)^{-11/6} e^{-f^2/f_i^2}, \tag{A-1}$$

where $C_n^2(z)$ is the structure constant which represents of the turbulence at each position z in the propagation. This model takes into account the inner and outer scale by incorporating $f_i = 1/l_0$ and $f_0 = 1/L_0$ in the equation, where l_0 and L_0 are called the the inner and outer scale. Since we will do a numerical implementation it is not necessary to incorporate the inner scale in the equation, because the dynamic range of the spectrum is so large that the effect of the roll-off due to the exponential term containing the inner scale will be negligible. Hence we can simplify our equation to:

$$\Phi(f,z) = 0.033C_n^2(z)(f^2 + f_0^2)^{-11/6} \tag{A-2}$$

Using Fried's coherence length:

$$r_0 = \left[\frac{0.423f^2}{cos(\gamma)} \int C_n^2(z)dz\right]^{-3/5} \tag{A-3}$$

Now we can switch to a notation using Fried's coherence for the power spectral density of the atmospheric turbulence.

$$\Phi(f) = 0.023r_0^{-5/3}(f^2 + f_0^2)^{-11/6} \tag{A-4}$$

From here on we will discuss how exactly we can produce a phase screen using the equation above. For random processes, we can create a realization by filtering Gaussian white noise using the amplitude spectrum as a filter, which is the square root of the power spectral density. Using the inverse Fourier transform we will obtain the phase screen. Expressed in equation form this looks like:

$$\phi(r) = \iint_{-\infty}^{\infty} n(f)\sqrt{\Phi(f)}e^{ir\cdot f}df, \tag{A-5}$$

where $n(f)$ is complex Gaussian white noise with zero mean and standard deviation of one. Our first step towards using a FFT algorithm will be to discretize this expression:

$$\phi(r) = \sum_{f_x}\sum_{f_y} n(f_x,f_y)\sqrt{\Phi(f_x,f_y)}e^{i2\pi(f_x x + f_y y)}\Delta f_x \Delta f_y \tag{A-6}$$

Since it is not possible to take an infinite number of samples we will have to limit our support width and number of samples.

$$\phi(r) = \sum_{f_x=-N_x/2}^{Nx/2-1}\sum_{f_y=-Ny/2}^{Ny/2-1} n(f_x,f_y)\sqrt{\Phi(f_x,f_y)}\frac{1}{G_x G_y}e^{i2\pi(f_x x/N_x + f_y y/N_y)} \tag{A-7}$$

This can be implemented easily with an FFT algorithm to obtain a phase screen.

A-1 Important properties of the spectral power spectrum method

The first important problem is that the Fourier transform will result in a periodic realization. This will not be a problem as long as we take into account that a limited amount of data from the history should be considered for identification and control.

The second problem is somewhat more important and restricting. It is an inherent limitation of the chosen method that the minimum and maximum frequencies are settled. As such, the

minimum frequency is $f_{min} = 1/L$, where L is the screen-size. Therefore, if no cautions are made, low spatial frequencies might be inadequately captured with this method.

This can be understood better from Figure A-1 where we have picked a numerical example of the amplitude spectrum. As can be seen there is a lot of energy stored in the low frequency part with a finite outer scale of 100 m. When we assume our telescope to have a diameter of 1 m and we choose to produce only for this support width, the first sample will start from $f = 1m^{-1}$. Even if we try to generate a phase screen of 10 by 10 m, the first covered frequency would be $f = 0.1\ m^{-1}$, which is still inadequate sampling of the low frequency content.

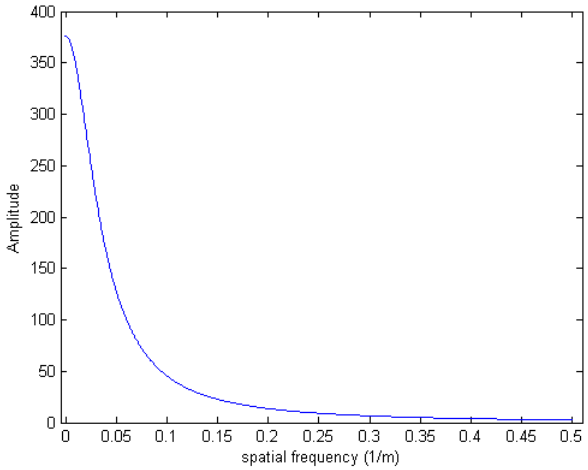

Figure A-1: A 1-D slice of the amplitude spectrum with $r_0 = 0.15m$ and $L_0 = 100m$.

Unfortunately, choosing to dismiss the low-frequency information is not an option, because in the simulation we would miss important turbulence characteristics such as tip and tilt, which are encoded in the low-frequency part. The easiest solution to overcome this problem is to produce a large enough screen and extract a small portion from it. This will contain also the subharmonics for that small part of the screen, because we have ensured that we sample the chosen outer scale correctly, which determines the low-frequency characteristics. In [58] a rule of thumb is used for the chosen screen size. In order to adequately sample the low-frequency content, the screen should be five times larger than the outer scale.

There are also several different methods are available to overcome this problem [58] [59] [57]. These methods basically use irregular sampling to overcome the problem of not being able to sample the low-frequency content correctly. As one can imagine, it would already suffice to use a finer sampling in the low-frequency zone while using a rougher sampling in the high-frequency zone where almost no energy is stored.

A-1-1 Evaluation of the obtained phase screen

After obtaining the phase screen, we have to evaluate and compare which one is better. This is done by calculating the average spectral power density of the realization and comparing it to the theoretical version. For this purpose, we will use the WienerâĂŞKhinchin theorem. This allows to compute the auto-correlation and therewith the power spectral density from the raw data:

$$F_R(fx, fy) = FFT2(\phi(x, y)) \tag{A-8}$$
$$PSD(fx, fy) = F_R(fx, fy)F_R*(fx, fy) \tag{A-9}$$

First we will compare the method of taking a larger screen without decreasing the sample rate. This means a significant increase in calculation time. For the purpose of evaluation of the method, we took a 1-D cross-section of the screen of 655.36 m and 65536 samples in both dimensions, we took the average power spectral density of realization that are 10 by 10 m. The size of 10 m is chosen, because of the fact that a smaller screen size would produce a power spectral density with insufficient number of samples to make any important conclusions. The result of theory versus realization can be found in Figure A-2.

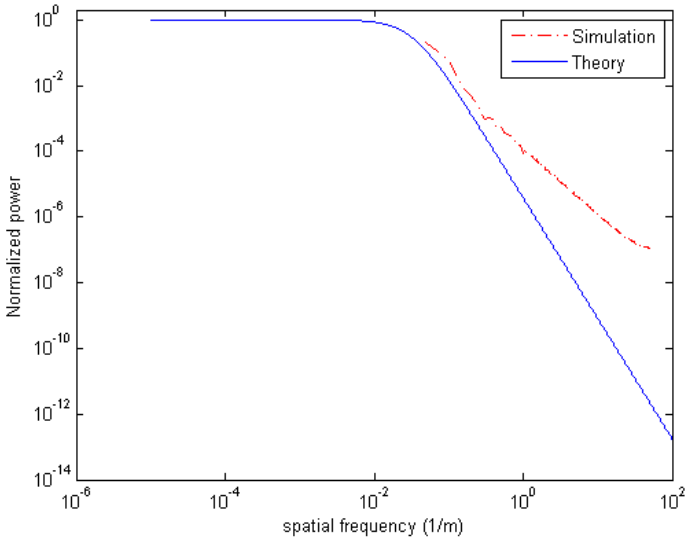

Figure A-2: Spectrum of atmospheric turbulence: theory versus simulation of 655.36 m.

Although the result of A-2 shows good results, the first roll-off point is not so good visible due to the limited size of the screen. Therefore, since we are evaluating in a single dimension, we produced a 1-D phase screen using the same method, but with a much larger screen length of 335 km. This shows us clearly that the low-frequency behavior of the phase screen used in our simulation has the correct characteristics.

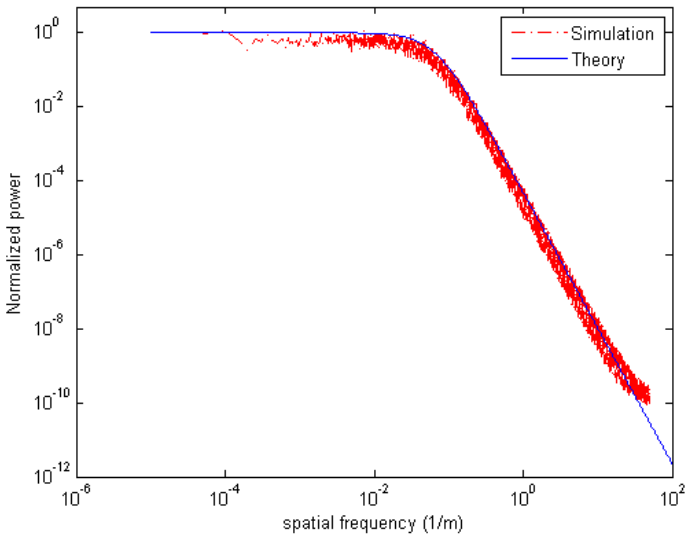

Figure A-3: Spectrum of atmospheric turbulence: theory versus simulation of 335 km.

Appendix B

Notions of identifiability and informativity for prediction error identification

B-1 Notion of identifiability

Let us assume a system that is defined by a model structure which is parametrized by a vector $\theta \in \mathcal{R}^d$:

$$y(t) = G(q^{-1}, \theta)u(t) + H(q^{-1}, \theta)e(t) \tag{B-1}$$

A certain $\theta \in \mathcal{R}^d$ gives a model $M(\theta) = [G(q^{-1}, \theta), \quad H(q^{-1}, \theta)]$. We will also define a model structure $\mathcal{M}$ as being a differentiable mapping from a connected open subset $D_\theta \in \mathcal{R}^d$ to a model set $\mathcal{M}^*$ [60]:

$$\mathcal{M} : \theta \in D_\theta \rightarrow M(\theta) = [G(q^{-1}, \theta), \quad H(q^{-1}, \theta)] \in \mathcal{M}^* \tag{B-2}$$

If a model structure $\mathcal{M}(\theta)$ is identifiable at some value θ_0 then it means that the model $[G(\theta_0), H(\theta_0))]$ cannot be represented by any other $[G(\theta), H(\theta))] \in \mathcal{M}$.

For a more mathematical definition of identifiability, we shall first introduce some new notations for the earlier defined expressions of the one-step-ahead predictor:

$$\hat{y}(k|k-1, \theta) = H^{-1}(\theta)G(\theta)u(k) + [I - H^{-1}(\theta)]y(k) \tag{B-3}$$

$$\hat{y}(k|k-1, \theta) = W_u(\theta)u(k) + W_y(\theta)y(k), \tag{B-4}$$

where $W_u(\theta) = H^{-1}(\theta)G(\theta)$ and $W_y(\theta) = [I - H^{-1}(\theta)]$. We shall also introduce the following notations:

$$W(\theta)\widehat{=}[W_u(\theta) \quad W_y(\theta)], \quad z(k)\widehat{=}\begin{bmatrix}u(k)\\y(k)\end{bmatrix} \tag{B-5}$$

A parametric model structure $M(\theta)$ is locally identifiable at a value θ_0 if there exists a $\delta > 0$ such that for all θ in $||\theta - \theta_0|| \leq \delta$:

$$W(e^{j\omega}, \theta) = W(e^{j\omega}, \theta_0) \quad \forall\omega \Rightarrow \theta = \theta_0 \tag{B-6}$$

The model structure is globally identifiable at the given value θ_0 if the equation above holds for $\delta \to \infty$. When the equation above holds for any given $\theta_0 \in \mathcal{R}^d$, the model structure is said to be globally identifiable.

B-2 Notion of informativity

Not all experiments Z^N will allow to distinguish the model $[G(\theta_0), \quad H(\theta_0))]$ from all other possibilities in the model set $\mathcal{M}$. Therefore, the notion of informativity is introduced. A data set Z^N is defined to be informative with respect to the model set $\mathcal{M}$ if for any two models $W_1(q)$ and $W_2(q)$ within the set $\mathcal{M}$ if the following equation

$$\overline{E}[(W_1(\theta_1) - W_2(\theta_2))z(k)]^2 = 0, \tag{B-7}$$

holds if and only if $W_1 = W_2$ [34]. This is basically telling us that a data set is informative with respect to a model if and only if it can uniquely distinguish each member of the model set. If we define the following notation $W_1(\theta_1) - W_2(\theta_2) = [\Delta W_u(\theta_1, \theta_2) \quad \Delta W_y(\theta_1, \theta_2)]$ then the equation above can be rewritten as:

$$\overline{E}[\Delta W_u(\theta_1, \theta_2)u(k) + \Delta W_y(\theta_1, \theta_2)y(k)]^2 = 0 \tag{B-8}$$

Bibliography

[1] M. Born and E. Wolf, *Principles of optics: electromagnetic theory of propagation, interference and diffraction of light*. CUP Archive, 2000.

[2] J. Kalkman and S. Stallinga, "Lecture notes in imaging systems," December 2015.

[3] F. Roddier, *Adaptive optics in astronomy*. Cambridge university press, 1999.

[4] C. A. Roddier and F. J. Roddier, "New optical testing methods developed at the university of hawaii: results on ground-based telescopes and hubble space telescope," in *8th Intl Symp on Gas Flow and Chemical Lasers*, pp. 37–43, International Society for Optics and Photonics, 1992.

[5] P. Mercère, P. Zeitoun, M. Idir, S. Le Pape, D. Douillet, X. Levecq, G. Dovillaire, S. Bucourt, K. A. Goldberg, P. P. Naulleau, *et al.*, "Hartmann wave-front measurement at 13.4 nm with λ euv/120 accuracy," *Optics letters*, vol. 28, no. 17, pp. 1534–1536, 2003.

[6] C. Smith, R. Marinică, A. Den Dekker, M. Verhaegen, V. Korkiakoski, C. Keller, and N. Doelman, "Iterative linear focal-plane wavefront correction," *JOSA A*, vol. 30, no. 10, pp. 2002–2011, 2013.

[7] M. J. Booth, D. Débarre, and A. Jesacher, "Adaptive optics for biomedical microscopy," *Optics and Photonics News*, vol. 23, no. 1, pp. 22–29, 2012.

[8] C. O. Molins and J. Rebling, *Adaptive Optics for Microscopy*. PhD thesis, Polytechnic University of Catalonia, 2013.

[9] T. Van Werkhoven, J. Antonello, H. Truong, M. Verhaegen, H. Gerritsen, and C. Keller, "Snapshot coherence-gated direct wavefront sensing for multi-photon microscopy," *Optics express*, vol. 22, no. 8, pp. 9715–9733, 2014.

[10] P. Godara, A. M. Dubis, A. Roorda, J. L. Duncan, and J. Carroll, "Adaptive optics retinal imaging: emerging clinical applications," *Optometry and vision science: official publication of the American Academy of Optometry*, vol. 87, no. 12, p. 930, 2010.

[11] J. Kolb, P.-Y. Madec, M. Le Louarn, N. Muller, and C. Béchet, "Calibration strategy of the aof," in *SPIE Astronomical Telescopes+ Instrumentation*, pp. 84472D–84472D, International Society for Optics and Photonics, 2012.

[12] C. Béchet, M. Tallon, and É. Thiébaut, "Optimization of adaptive optics correction during observations: Algorithms and system parameters identification in closed-loop," in *SPIE Astronomical Telescopes+ Instrumentation*, pp. 84472C–84472C, International Society for Optics and Photonics, 2012.

[13] R. K. Tyson, *Principles of adaptive optics*. CRC press, 2015.

[14] G. K. Batchelor, *The theory of homogeneous turbulence*. Cambridge university press, 1953.

[15] A. Kolmogorov, S. Friedlander, and L. Topper, "Turbulence: Classic papers on statistical theory," *Interscience*, 1961.

[16] V. P. Lukin, *Atmospheric adaptive optics*. SPIE Press, 1995.

[17] V. I. Tatarskii, "Wave propagation in turbulent medium," *Wave Propagation in Turbulent Medium, by Valerian Ilich Tatarskii. Translated by RA Silverman. 285pp. Published by McGraw-Hill, 1961.*, vol. 1, 1961.

[18] S. E. Egner, *Multi-Conjugate Adaptive Optics for LINC-NIRVANA: Laboratory Tests of a Ground-Layer Adaptive Optics System and Virtical Turbulence Measurements at Mt. Graham*. PhD thesis, Combined Faculties for the Natural Sciences and for Mathematics of the Ruperto-Carola University of Heidelberg, Germany, 2006.

[19] R. V. Shack and B. Platt, "Production and use of a lenticular hartmann screen," in *Journal of the Optical Society of America*, vol. 61, p. 656, 1971.

[20] F. Roddier, "Curvature sensing and compensation: a new concept in adaptive optics," *Applied Optics*, vol. 27, no. 7, pp. 1223–1225, 1988.

[21] R. Ragazzoni, "Pupil plane wavefront sensing with an oscillating prism," *Journal of modern optics*, vol. 43, no. 2, pp. 289–293, 1996.

[22] J. Hartmann, *Bemerkungen über den Bau und die Justirung von Spektrographen*. Springer, 1900.

[23] J. Hartmann, *Objektivuntersuchungen*. Springer, 1904.

[24] Spiricon, *Hartmann Wavefront Analyzer Tutorial*, 2004.

[25] R. H. Hudgin, "Wave-front reconstruction for compensated imaging," *JOSA*, vol. 67, no. 3, pp. 375–378, 1977.

[26] D. L. Fried, "Least-square fitting a wave-front distortion estimate to an array of phase-difference measurements," *JOSA*, vol. 67, no. 3, pp. 370–375, 1977.

[27] W. H. Southwell, "Wave-front estimation from wave-front slope measurements," *JOSA*, vol. 70, no. 8, pp. 998–1006, 1980.

[28] L. A. Poyneer, D. T. Gavel, and J. M. Brase, "Fast wave-front reconstruction in large adaptive optics systems with use of the fourier transform," *JOSA A*, vol. 19, no. 10, pp. 2100–2111, 2002.

[29] L. Gilles, C. R. Vogel, and B. L. Ellerbroek, "Multigrid preconditioned conjugate-gradient method for large-scale wave-front reconstruction," *JOSA A*, vol. 19, no. 9, pp. 1817–1822, 2002.

[30] M. Rosensteiner, "Cumulative reconstructor: fast wavefront reconstruction algorithm for extremely large telescopes," *JOSA A*, vol. 28, no. 10, pp. 2132–2138, 2011.

[31] C. C. de Visser and M. Verhaegen, "Wavefront reconstruction in adaptive optics systems using nonlinear multivariate splines," *JOSA A*, vol. 30, no. 1, pp. 82–95, 2013.

[32] A. Chiuso, R. Muradore, and E. Marchetti, "Dynamic calibration of adaptive optics systems: A system identification approach," *Control Systems Technology, IEEE Transactions on*, vol. 18, no. 3, pp. 705–713, 2010.

[33] T. Söderström and P. Stoica, *System identification*. Prentice-Hall, Inc., 1988.

[34] L. Ljung, *System identification: Theory for the user*. Prentice-Hall Inc., 1987.

[35] L. Ljung, *System identification: Theory for the user*. Springer, 1998.

[36] P. Van den Hof, "Closed-loop issues in system identification," *Annual reviews in control*, vol. 22, pp. 173–186, 1998.

[37] K. Lindqvist, *On experiment design in identification of smooth linear systems*. PhD thesis, Signaler, sensorer och system, 2001.

[38] X. Bombois, G. Scorletti, M. Gevers, P. M. Van den Hof, and R. Hildebrand, "Least costly identification experiment for control," *Automatica*, vol. 42, no. 10, pp. 1651–1662, 2006.

[39] L. Mišković, A. Karimi, D. Bonvin, and M. Gevers, "Closed-loop identification of multivariable systems: With or without excitation of all references?," *Automatica*, vol. 44, no. 8, pp. 2048–2056, 2008.

[40] X. Bombois, G. Scorletti, P. Van den Hof, and M. Gevers, "Least costly identification experiment for control. a solution based on a high-order model approximation," in *Proc. American Control Conference, Boston*, 2004.

[41] H. Hjalmarsson, "From experiment design to closed-loop control," *Automatica*, vol. 41, no. 3, pp. 393–438, 2005.

[42] C. Pearson, *Handbook of applied mathematics: selected results and methods*. Springer Science & Business Media, 2012.

[43] X. Bombois and G. Scorletti, "Design of least costly identification experiments: The main philosophy accompanied by illustrative examples," *Journal Européen des Systèmes Automatisés*, vol. 46, no. 6-7, pp. 587–610, 2012.

[44] S. Boyd, "Robust control tools: Graphical user-interfaces and lmi algorithms," tech. rep., STANFORD UNIV CA DEPT OF ELECTRICAL ENGINEERING, 1994.

[45] M. Gevers, "A personal view of the development of system identification: A 30-year journey through an exciting field," *IEEE Control Systems*, vol. 26, no. 6, pp. 93–105, 2006.

[46] P. M. Harrington and B. M. Welsh, "Frequency-domain analysis of an adaptive optical system's temporal response," *Optical Engineering*, vol. 33, no. 7, pp. 2336–2342, 1994.

[47] N. Doelman. personal communication.

[48] M. Barenthin, H. Jansson, and H. Hjalmarsson, "Applications of mixed h 2 and h infin; input design in identification," *IFAC Proceedings Volumes*, vol. 38, no. 1, pp. 458–463, 2005.

[49] D. E. Rivera, H. Lee, M. W. Braun, and H. D. Mittelmann, "Plant-friendly system identification: a challenge for the process industries," in *13th IFAC Symposium on System Identification (SYSID 2003)*, pp. 917–922, 2003.

[50] L. Gerencsér, H. Hjalmarsson, and J. Mårtensson, "Identification of arx systems with non-stationary inputsâĂŤasymptotic analysis with application to adaptive input design," *Automatica*, vol. 45, no. 3, pp. 623–633, 2009.

[51] C. R. Rojas, J. S. Welsh, G. C. Goodwin, and A. Feuer, "Robust optimal experiment design for system identification," *Automatica*, vol. 43, no. 6, pp. 993–1008, 2007.

[52] H. Hjalmarsson, J. Mårtensson, and B. Wahlberg, "On some robustness issues in input design," *IFAC Proceedings Volumes*, vol. 39, no. 1, pp. 511–516, 2006.

[53] C. R. Rojas, J.-C. Aguero, J. S. Welsh, G. C. Goodwin, and A. Feuer, "Robustness in experiment design," *IEEE Transactions on Automatic Control*, vol. 57, no. 4, pp. 860–874, 2012.

[54] M. van Dam, "Lecture notes - simulation of adaptive optics systems," July 2003.

[55] R. Fraanje, "Lecture notes - turbulence modeling," May 2011.

[56] B. L. McGlamery, "Computer simulation studies of compensation of turbulence degraded images," in *Image processing*, pp. 225–233, International Society for Optics and Photonics, 1976.

[57] E. M. Johansson and D. T. Gavel, "Simulation of stellar speckle imaging," in *1994 Symposium on Astronomical Telescopes & Instrumentation for the 21st Century*, pp. 372–383, International Society for Optics and Photonics, 1994.

[58] B. J. Herman and L. A. Strugala, "Method for inclusion of low-frequency contributions in numerical representation of atmospheric turbulence," in *OE/LASE'90, 14-19 Jan., Los Angeles, CA*, pp. 183–192, International Society for Optics and Photonics, 1990.

[59] R. Lane, A. Glindemann, J. Dainty, *et al.*, "Simulation of a kolmogorov phase screen," *Waves in random media*, vol. 2, no. 3, pp. 209–224, 1992.

[60] A. S. Bazanella, M. Gevers, and L. Mišković, "Closed-loop identification of mimo systems: a new look at identifiability and experiment design," in *Control Conference (ECC), 2007 European*, pp. 5694–5699, IEEE, 2007.